

SANDIA REPORT

SAND2008-5411

Unlimited Release

Printed August 2008

Public Release of Optimization of Metallization Scheme for Thin Emitter Wrap-Through Solar Cells for Higher Efficiency, Reduced Precious Metal Costs, and Reduced Stress

Peter Hacke, Jason Dominguez, David Meakin, Brian Murphy, and Douglas Ruby

Prepared by
Sandia National Laboratories
Albuquerque, New Mexico 87185 and Livermore, California 94550

Sandia is a multiprogram laboratory operated by Sandia Corporation, a Lockheed Martin Company, for the United States Department of Energy's National Nuclear Security Administration under Contract DE-AC04-94AL85000.

Approved for public release; further dissemination unlimited.

Issued by Sandia National Laboratories, operated for the United States Department of Energy by Sandia Corporation.

NOTICE: This report was prepared as an account of work sponsored by an agency of the United States Government. Neither the United States Government, nor any agency thereof, nor any of their employees, nor any of their contractors, subcontractors, or their employees, make any warranty, express or implied, or assume any legal liability or responsibility for the accuracy, completeness, or usefulness of any information, apparatus, product, or process disclosed, or represent that its use would not infringe privately owned rights. Reference herein to any specific commercial product, process, or service by trade name, trademark, manufacturer, or otherwise, does not necessarily constitute or imply its endorsement, recommendation, or favoring by the United States Government, any agency thereof, or any of their contractors or subcontractors. The views and opinions expressed herein do not necessarily state or reflect those of the United States Government, any agency thereof, or any of their contractors.

Printed in the United States of America. This report has been reproduced directly from the best available copy.

Available to DOE and DOE contractors from
U.S. Department of Energy
Office of Scientific and Technical Information
P.O. Box 62
Oak Ridge, TN 37831

Telephone: (865) 576-8401
Facsimile: (865) 576-5728
E-Mail: reports@adonis.osti.gov
Online ordering: <http://www.osti.gov/bridge>

Available to the public from
U.S. Department of Commerce
National Technical Information Service
5285 Port Royal Rd.
Springfield, VA 22161

Telephone: (800) 553-6847
Facsimile: (703) 605-6900
E-Mail: orders@ntis.fedworld.gov
Online order: <http://www.ntis.gov/help/ordermethods.asp?loc=7-4-0#online>



Public Release of Optimization of Metallization Scheme for Thin Emitter Wrap-Through Solar Cells for Higher Efficiency, Reduced Precious Metal Costs, and Reduced Stress

Peter Hacke, Jason Dominguez,
David Meakin, and Brian Murphy¹
Advent Solar, Inc.
5600 University Blvd. SE
Albuquerque, New Mexico 87106

Douglas Ruby
Solar Technologies, 6337
Sandia National Laboratories
P.O. Box 5800
Albuquerque, New Mexico 87185-1127

Abstract

Back-contact crystalline-silicon photovoltaic solar cells and modules offer a number of advantages, including the elimination of grid shadowing losses, reduced cost through use of thinner silicon substrates, simpler module assembly, and improved aesthetics. While the existing edge tab method for interconnecting and stringing edge-connected back contact cells is acceptably straightforward and reliable, there are further gains to be exploited when you have both contact polarities on one side of the cell. In this work, we produce “busbarless” emitter wrap-through solar cells that use 41% of the gridline silver (Ag) metallization mass compared to the edge tab design. Further, series resistance power losses are reduced by extraction of current from more places on the cell rear, leading to a fill factor improvement of about 6% (relative) on the module level. Series resistance and current-generation losses associated with large rear bondpads and busbars are eliminated. Use of thin silicon (Si) wafers is enabled because of the reduced Ag metallization mass and by interconnection with conductive adhesives leading to reduced bow. The busbarless cell design interconnected with conductive adhesives passes typical International Electrotechnical Commission damp heat and thermal cycling tests.

¹ Summary of Work for Final Form Contract – 104-FCC (10-99). Period of work: 08/26/2006 to 12/31/2007. Reference document number: 616976.

CONTENTS

INTRODUCTION AND BACKGROUND	9
PROOF OF CONCEPT	13
Design Dielectric Pattern and Connector Pattern	14
Obtain Candidate Dielectric Material and Connector Materials.....	16
Dielectric Materials.....	16
Connector Materials.....	16
Research Method to Isolate Screen-Printed Busbars and High Series Resistance	
Areas of the Cell	18
Fabricate and Test Proof-of-Concept Cells.....	19
Achieving a Prototype 15% Busbarless Cell	22
PRODUCTION OF 125 mm × 125 mm BUSBARLESS CELLS	24
Engineering Design of 125 mm × 125 mm Busbarless Cells	24
Cell Design.....	24
Development of Cell Measurement Techniques.....	25
Stress Modeling	27
Single-Cell Accelerated Testing	29
PRODUCTION OF EWT CELL MINI-MODULES AND TEST	32
String and Encapsulate 12-Cell and Other Multi-Cell Laminates	32
Review of Bus Requirements and Candidates	32
String Fabrication.....	33
MODULE FABRICATION.....	34
Summary of Busbarless Mini-Module Test Results	35
Accelerated Testing of Multi-Cell Laminates.....	37
Thermal Cycling	37
Damp Heat	40
CONCLUSION.....	43

FIGURES

Figure 1. Front and rear of the 125 mm × 125 mm multicrystalline-Si EWT solar cell that is in pilot production.....	10
Figure 2. Differing fill factor ranges observed in current process with and without the series resistance associated with the busbars at the cell edges.	11
Figure 3. Cross section of the cell with n+ diffused regions shown in red and p-type Si regions shown in blue to illustrate the source series resistance associated with the busbar at the cell edge.	11
Figure 4. LBIC imaging over the p-busbar region of the cell indicating significantly reduced response from the infrared portion of the spectrum.....	12
Figure 5. Schematic illustration of “busbarless EWT” cell with interconnects.....	12
Figure 6. The screen-printed metallization of the existing 125 mm × 125 mm solar cell.	14
Figure 7. Schematic of dielectric used to electrically isolate alternating gridlines from subsequently connected copper ribbon bussing material.....	14
Figure 8. Solder bump screen pattern used to apply solder into the openings of the dielectric.....	15
Figure 9. Manual solder applicator being used to apply solder into the openings of the dielectric.....	15
Figure 10. Drop in fill factor after application of dielectric paste A.	16
Figure 11. Drop in pseudo fill factor (fill factor void of series resistance losses) after application of dielectric paste B.....	17
Figure 12. Bow associated with manually soldering copper ribbon conductors to the screen-printed silver gridlines.	17
Figure 13. A busbarless cell using conductive adhesive to connect the screen-printed Ag gridlines to the copper ribbon.	18
Figure 14. Demonstration of the increase in the non-ideal diode saturation current J_{o2} that occurs as the dielectric resist is applied and after the busbars are cut with the dicing saw (“wd” in figure axes).....	18
Figure 15. Demonstration of the increase in the non-ideal diode saturation current J_{o2} that occurs as the dielectric is applied and after the busbars are cut with the laser (“bb cut” in figure axes).....	19
Figure 16. Baseline cell at Stage 1 – with screen-printed and sintered Ag busbars and tabbing areas located at opposite extremities of the cell.....	20
Figure 17. Stage 2 – the screen-print dielectric material is applied to create vias for the contacts between the gridlines and the connecting ribbon, and to isolate the gridlines of opposite polarity.....	20
Figure 18. Screen-printed busbars are cut off with laser or dicing saw.....	21
Figure 19. Wire ribbons are manually connected to each gridline with conductive adhesive – three copper ribbons are used for each polarity.	21
Figure 20. Complete 125 mm × 125 mm prototype cell.....	23
Figure 21. Prototype busbarless cell with dielectric printed.....	24

Figure 22. Busbarless cell before dielectric print showing three rows of bussing pads for each polarity.....	24
Figure 23. Revised dielectric shown over p and n metal traces.....	25
Figure 24. Solid works rendering of jig with two probe bars in place.....	25
Figure 25. The probe jig is shown configured to measure a bussed cell.	26
Figure 26. Pogo probe bar with test leads attached.	26
Figure 27. Solid works drawing showing assembled copper ball jig on a cell.....	26
Figure 28. Copper ball test jig with center bars assembled.	27
Figure 29. Fill factor and cell efficiency of ball bearing EWT (BBEWT) cells measured with the copper ball bearing jig, for two different lots, as labeled.	27
Figure 30. Comparison of pull strength of cells bussed with adhesive 3 (left) and adhesive 1 (right).	28
Figure 31. Carlsbad cell tested in thermal cycle to access the effect of dielectric tape on cell performance.	30
Figure 32. Summary of tape dielectric effect on cell performance after 300 thermal cycles. The relative change R (%) is indicated.	30
Figure 33. Modified Carlsbad cell after 300 thermal cycles.....	31
Figure 34. Summary of modified Carlsbad BBEWT cells subjected to 300 thermal cycles. The relative change R (%) is indicated.	31
Figure 35. Results of pull test indicating pull force vs. displacement for various interconnects	32
Figure 36. Busbarless cell strings shown interconnected with wire cloth.	33
Figure 37. A 12-cell busbarless module.	34
Figure 38. Component cell performance parameters as measured by the ball bearing cell tester; string, module (before and after lamination) performance parameters measured with a QuickSun module tester.	35
Figure 39. Results of thermal cycling tests for mini-module 08132007-01: 3 x 4 cell module with ribbon, conductive adhesive.	37
Figure 40. Results of thermal cycling tests for mini-module 08132007-02: 3x3 cell module with ribbon, conductive adhesive.	38
Figure 41. Results of thermal cycling tests for mini-module 08172007-04:3x3 cell module with ribbon, conductive adhesive.	38
Figure 42. Results of thermal cycling tests for mini-module 7051608-4-8-18: 1x3 cell module with corrugate ribbon, conductive adhesive.	39
Figure 43. Results of thermal cycling tests for mini-module 7051607-4-5-6:1x3 cell module with ribbon, conductive adhesive.	39
Figure 44. Results of damp heat tests for mini-module 08132007-01:3x4 cell module with ribbon, conductive adhesive.....	40
Figure 45. Results of damp heat tests for mini-module 08132007-02: 3x3 cell module with ribbon, conductive adhesive.....	41

Figure 46. Results of damp heat tests for mini-module 08172007-04:3x3 cell module with ribbon, conductive adhesive.....	41
Figure 47. Results of damp heat tests for mini-module 7051608-4-8-18:1x3 cell module with ribbon, XCA80229HF conductive adhesive.....	42
Figure 48. Results of damp heat tests for mini-module 7051607-4-5-6:1x3 cell module with ribbon, conductive adhesive.....	42

TABLES

Table 1. Cell test results measured for the EWT cell before the start of the busbarless conversion, measured after printing of the dielectric and application of the copper ribbons, and measured after laser cutting of the busbars.....	22
Table 2. Efficiency measurement of three prototype busbarless cells.....	23
Table 3. Pull tests with various conductive adhesive materials.....	29
Table 4. Module test results for six minimodules produced with busbarless cells.....	36

INTRODUCTION AND BACKGROUND

Back-contact silicon (Si) solar cells represent the next generation in crystalline-silicon photovoltaic (c-Si PV) modules. The advantages of back-contact cells compared to conventional cells with grids on the front surface include improved efficiency from elimination of grid shadowing losses; reduced cost through use of thinner silicon substrates and simpler module assembly; and improved aesthetics. The back-contact emitter wrap-through (EWT) cell is one of the most attractive back-contact cell approaches. The EWT cell uses laser-drilled holes in the silicon substrate to wrap the emitter from the front surface to the rear surface. It thereby completely eliminates grid obscuration losses. Much of the device consists of an n^+pn^+ structure where current is collected on both surfaces, which is advantageous for materials with modest diffusion lengths. EWT cells can use thinner silicon substrates because it avoids the stressful aluminum (Al)-alloyed back-surface field step. Another important advantage of the back-contact EWT cells is that it can be manufactured using industry-standard materials (e.g., p-type multicrystalline-silicon substrates), equipment (e.g., screen printers), and processes (e.g., PECVD silicon nitride passivation) – which helps reduce technical risk, reduces time to market, and allows the technology to ride the same technology evolution path of the bulk of the c-Si PV industry.

The baseline cell process uses a simple process sequence with a homogeneous emitter and a grid geometry that brings the current to the cell edges (Figure 1). The multicrystalline-silicon (mc-Si) EWT cells have median efficiencies around 15% (125 mm × 125 mm) without texturing and about 15.5% with texturing. The EWT cells typically use p-type mc-Si wafers that are laser-machined with holes in a 2 mm × 0.5 mm array. A dielectric that functions as a diffusion barrier to phosphorus is screen-printed on the rear to isolate the subsequently defined p and n regions and contacts on the back surface. The diffusion is carried out in $POCl_3$ to create an emitter over the front, back, and hole surfaces. Silicon nitride is deposited on the front and back surfaces to passivate the surfaces and as an antireflection coating on the front surface. Screen-printed silver (Ag) is used to contact to the p-type base, n^+ emitter, and for the conductive grid. This process has a similar level of complexity, and therefore cost, as the standard Al-alloyed back-surface field cells that are commonly produced today.²

The 125 mm × 125 mm EWT cell geometry (Figure 1) uses relatively thick (>40 μ m) printed Ag grids. The thick conductor is required due to the geometry where the current must be transported the full length of the solar cell. An even thicker Ag layer would be required for a larger area (156 × 156-mm-square) solar cell using this same geometry. The thick Ag introduces stress due to differences in thermal expansion coefficients, which induces bowing of the cell. The increasing Ag cost is also a substantial issue. The stress and bowing issues obviously become more substantial for thinner substrates and for larger-area solar cells.

Unlike conventional solar cells where the current collecting busbars are on the front of the cell shading the region below it, the busbars on the EWT cell are on the rear. The Si area over the rear busbar is active in the EWT cell. Over the busbars, photogenerated positive and negative carriers must both reach their respective terminals to obtain the maximum available power from the cell—this distance could be quite long, resulting in a power loss due to series resistance.

² J. M. Gee, et al., “Towards a manufacturable back-contact emitter-wrap-through solar cell, *IEEE Photovoltaic Specialists Conf.*, January 2004 (Orlando, FL).

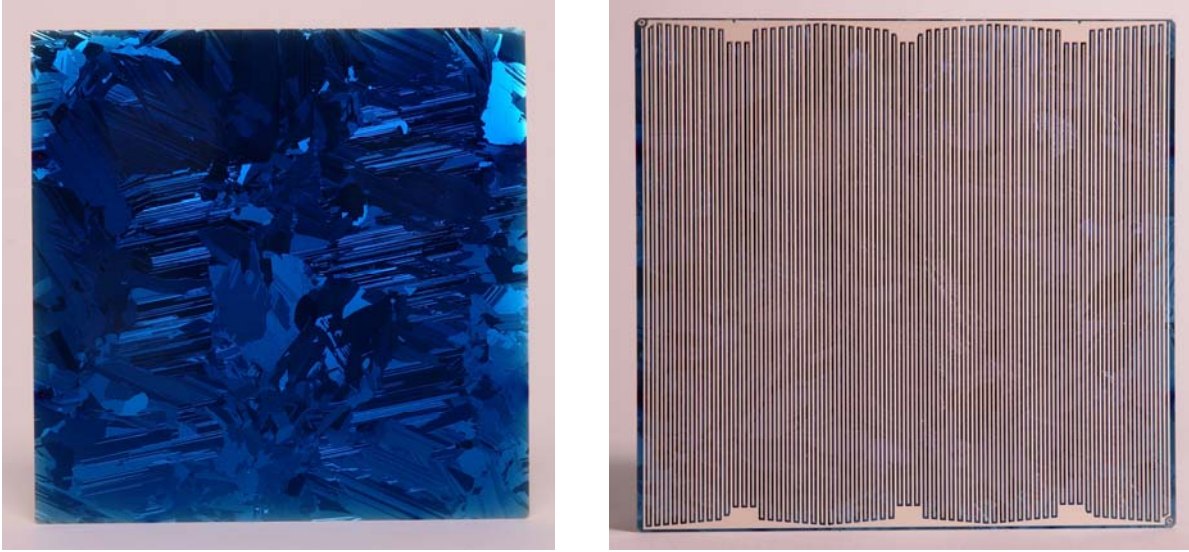


Figure 1. Front and rear of the 125 mm \times 125 mm multicrystalline-Si EWT solar cell that is in pilot production. The front surface is free of any metal gridline or busbar obscuration leading to excellent aesthetics. On the rear surface, interdigitated grid fingers leading to the positive and negative polarity busbars and contact pads can be seen. Over the active area of the cell, micro through-holes allow current collection from the front of the cell to the rear grid.

When the area over the busbar of the EWT cell is masked, the series resistance (R_s) of the remaining active area is comparatively lower and the fill factor higher than the whole cell that includes the busbars (Figure 2).³ This is mainly due to the series resistance over the expanse of the busbar (Figure 3). Further, laser-beam-induced current (LBIC) indicates significantly degraded infrared response over p-type regions, including the p-busbar, reducing the current output of the cell (Figure 4). A method to reduce or eliminate these series resistance and current losses associated with the rear-mounted busbars must therefore be found.

The purpose of this work is to develop key processes to improve efficiency, reduce cell thickness, and increase cell size. In particular, this project will examine alternative metallization technologies and geometries that reduce the cost of the metallization, reduce the stress induced by the metallization, reduce the series resistance associated with the current-collection grid, and can be scaled to larger and thinner solar cells. The primary approach is an alternative geometry for interconnecting the back-contact EWT cell where the current is extracted from multiple points in the interior of the solar cell (Figure 5).

³ D. D. Smith, J. M. Gee, M. D. Bode, and J. C. Jimeno, *IEEE Trans. Electron Devices*, (46) 1999.

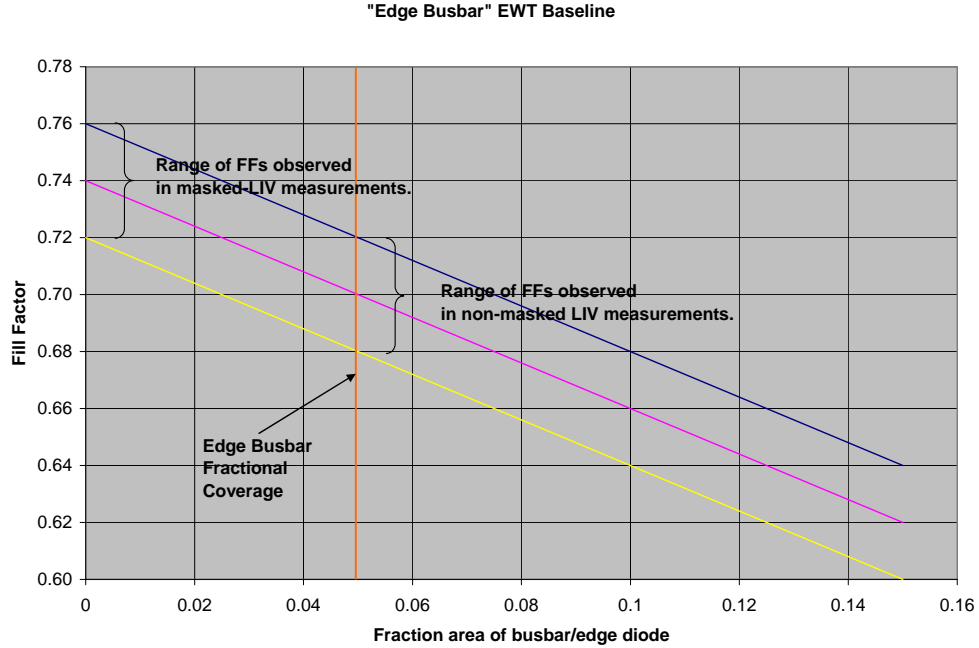


Figure 2. Differing fill factor ranges observed in current process with and without the series resistance associated with the busbars at the cell edges. The series resistance of the busbars is eliminated from the circuit in the “masked-illuminated current-voltage (Lighted I vs. V) (LIV)” measurement. We typically observe values between 0.72 and 0.75 in masked-LIV measurement. A maximum value of 0.76 is estimated for the masked-LIV based on further reductions in series resistance, R_s .

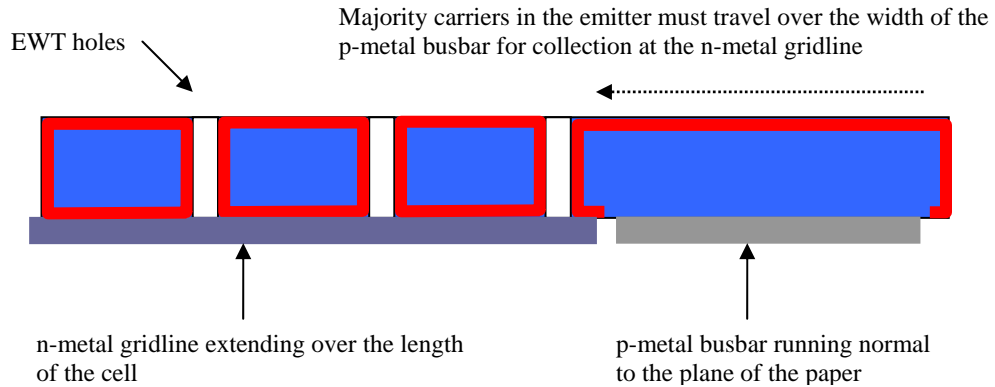


Figure 3. Cross section of the cell with n^+ diffused regions shown in red and p -type Si regions shown in blue to illustrate the source series resistance associated with the busbar at the cell edge. The spacing between the EWT holes is 0.5 mm whereas the region on the right over the p -busbar and tabs ranges from 2 mm to 8 mm as the busbar is tapered.

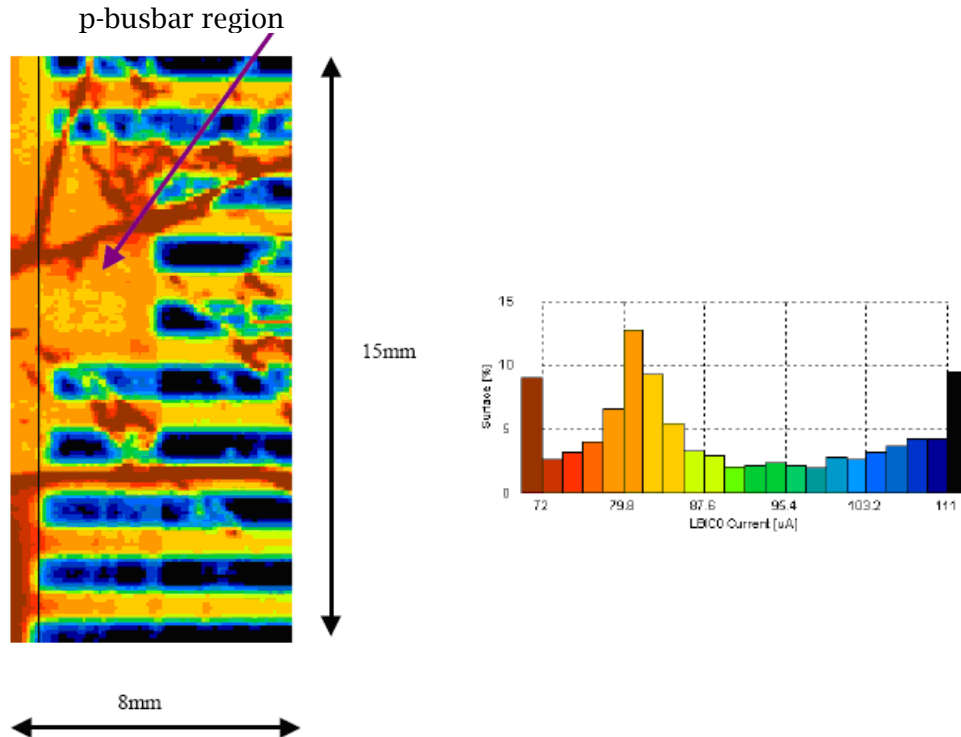


Figure 4. LBIC imaging over the p-busbar region of the cell indicating significantly reduced response from the infrared portion of the spectrum.

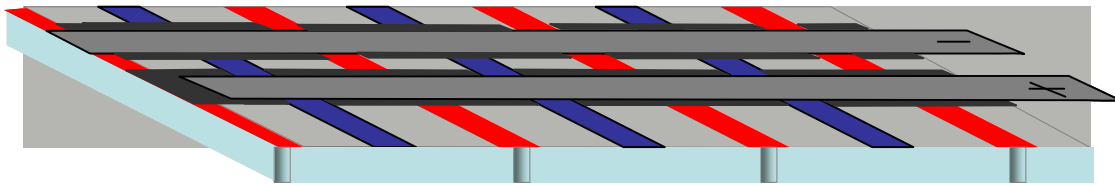


Figure 5. Schematic illustration of “busbarless EWT” cell with interconnects. The red and blue traces represent the negative- and positive-polarity grids, respectively. The grey layer represents the interconnect ribbons between solar cells. The black layer is an insulator patterned to isolate the interconnect ribbons from the gridlines of the opposite polarity.

This method achieves a reduction in series resistance through extraction of current at more locations on the cell rear and a reduction in the amount of screen-printed metal applied to the silicon to reduce stress and reduce Ag cost. This approach also scales to larger-area cell sizes more easily. This will be achieved by increasing the active area of the cell through removal of the screen-printed busbars and replacing them with metallization applied to the back of the cell that connects to each grid finger. Candidate materials and processes for the connection between the gridlines and the ribbon and the ribbon material itself will be selected and tested. Cell interconnection (stringing) techniques for the new cell metallization will be designed and applied. Finally, accelerated lifetime testing must be performed with cells that are encapsulated into modules to determine the best materials and designs for the new EWT cell and module to be demonstrated in this work.

PROOF OF CONCEPT

The goal of the proof-of-concept stage of this work was the demonstration of a 15% busbarless EWT cell and demonstration of fill-factor gain when a conventional edge-tab cell is modified into a busbarless cell.

The basic steps to we carried out for obtaining proof-of-concept cells are as follows:

1. Obtain existing 125 mm × 125 mm baseline EWT cells (referred to as “Carlsbad” cells) and their cell test information from the pilot line.
2. Screen-print dielectric material to create vias for the contacts between the gridlines and the connecting ribbon and to isolate the gridlines of opposite polarity.
3. Screen-print or manually apply solder paste or other conductor at the vias for the contacts between the gridlines and the connecting ribbon.
4. Manually connect wire ribbons to each gridline—a ribbon for each polarity.
5. Cut off screen-printed busbars.
6. Test the modified cell.

To carry out these steps, the following procedures were carried out.

- ***Design dielectric pattern and connector pattern*** – Design and fabricate screens, stencils, or applicator tools to apply the dielectric materials, solder pastes, or conductive adhesives.
- ***Obtain candidate dielectric material and connector materials*** – Research and obtain sample dielectric materials to create vias for the contacts between the gridlines and the connecting ribbon and to isolate the gridlines of opposite polarity. Research and sample solder paste or other conductive adhesive for the contacts between the gridlines and the connecting ribbon.
- ***Research method to isolate screen-printed busbars and high series resistance areas of the cell*** – Test performance and practicality of methods such as dicing saw and laser cutting to remove the high series resistance areas of the baseline cell.
- ***Fabricate and test proof of concept cells*** – Test performance of dielectric and interconnect materials by fabricating proof-of-concept cells. Demonstrate the proof of concept by showing conversion efficiency gain of cell.
- ***Select materials for prototype cell design*** – Select candidate designs and material classes of dielectrics, interconnect materials, and laser micro through-hole configurations. Perform calculations to estimate required gridline dimensions, location, and type of ribbon materials.

Design Dielectric Pattern and Connector Pattern

A pattern for depositing a thick-film dielectric was designed and fabricated. A design that involves three pairs of ribbon tabs was designed to fit on top of the existing 125 mm \times 125 mm cell pattern to alternately isolate the p and the n gridlines. The existing 125 mm \times 125 mm cell's screen-printed metallization appears in Figure 6.

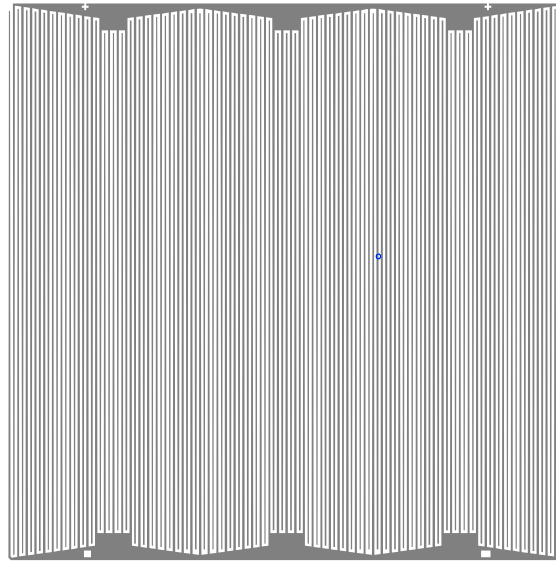


Figure 6. The screen-printed metallization of the existing 125 mm \times 125 mm solar cell. This conventional EWT cell design involves screen-printed busbars and tabs.

The screen-printed dielectric that was designed to isolate alternating polarity gridlines is shown in Figure 7.

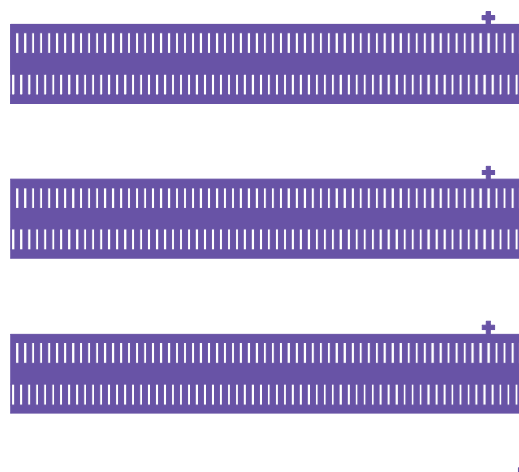


Figure 7. Schematic of dielectric used to electrically isolate alternating gridlines from subsequently connected copper ribbon bussing material.

For connecting the screen printed sintered Ag to the copper ribbon bussing material, we tried two methods. First we tried to screen-print solder paste into the openings of the dielectric. The screen-printed solder paste pattern is shown in Figure 8. This technique did not yield enough solder material into the openings of the dielectric and numerous open circuits were found after reflowing when trying to connect the screen-printed sintered Ag gridlines to the copper ribbon. We then used a hand-operated solder paste applicator nozzle to deposit solder paste into the openings of the dielectric (Figure 9). By this means, we could obtain more reliable contacts.



Figure 8. Solder bump screen pattern used to apply solder into the openings of the dielectric.

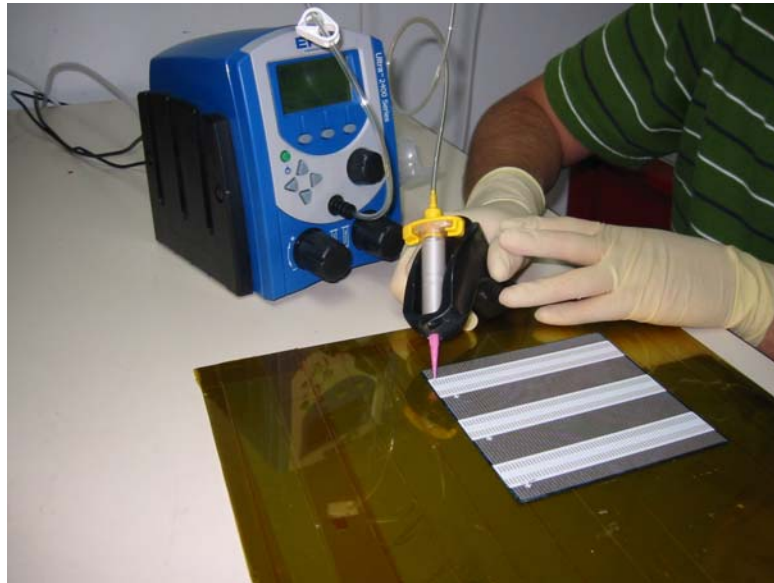


Figure 9. Manual solder applicator being used to apply solder into the openings of the dielectric.

Obtain Candidate Dielectric Material and Connector Materials

A study was carried out to determine materials that would perform acceptably as dielectrics and connector materials to conduct current from the Ag gridlines to the copper ribbon.

Dielectric Materials

We unfortunately found a drop in fill factor after application of almost all dielectric materials that we tested. Fill factor measured before and after the application of the dielectric is shown for two differing dielectric materials below (Figures 10 and 11).

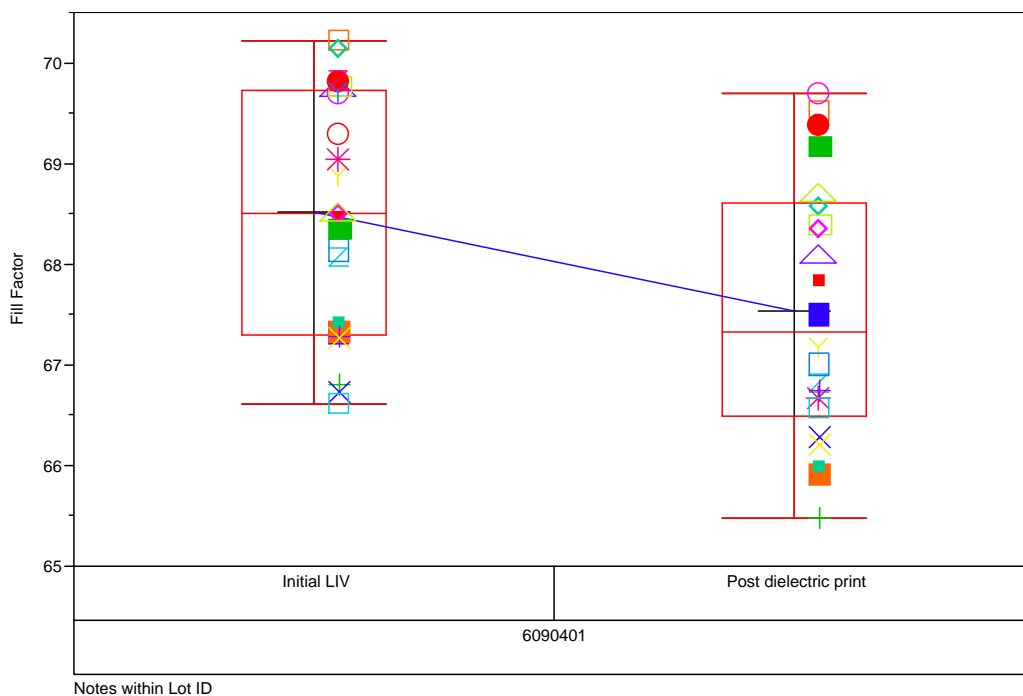


Figure 10. Drop in fill factor after application of dielectric paste A.

The drop in fill factor of about 0.01 as seen in Figures 10 and 11 leads to a calculated efficiency loss of about 0.2% absolute. Despite these losses in all dielectrics that we tested, we continued to build dielectric prototype busbarless cells.

Connector Materials

Several solder materials and several conductive adhesive materials were tested to connect the screen-printed sintered Ag gridlines to the copper ribbon. We tested the lead-free solder (96.5/3.0/0.5 SnAgCu alloy) and conventional 63/37 PbSn alloy. In both instances, solder bonding could successfully be carried out; however, the bow associated with the mismatch in temperature coefficients of expansions between the copper and the cell led to severe bowing of the cell (Figure 12).

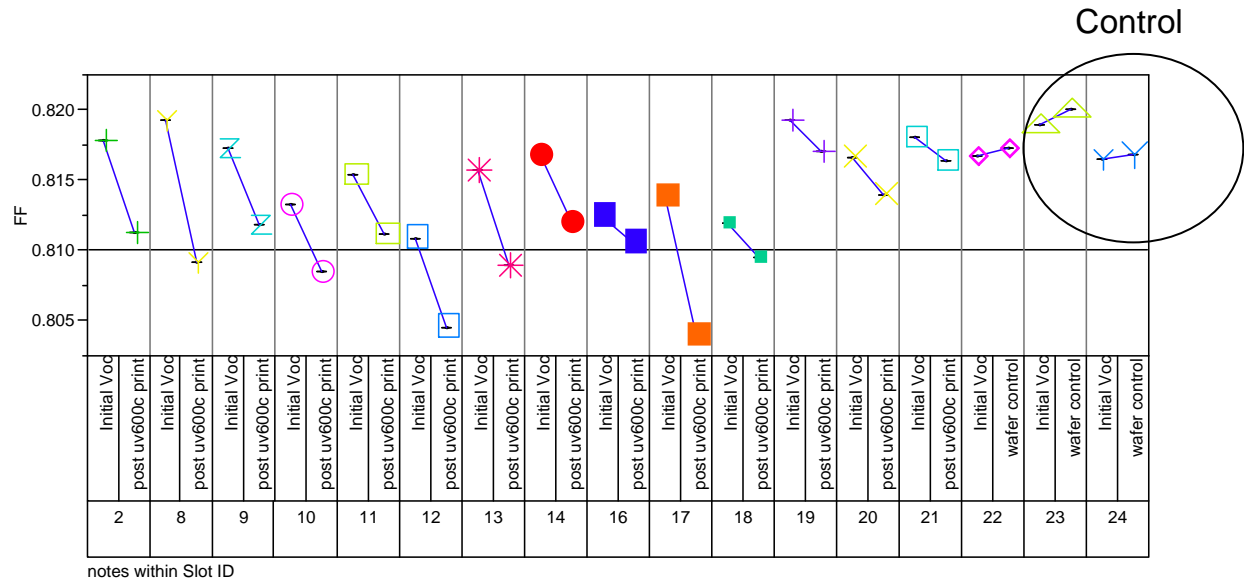


Figure 11. Drop in pseudo fill factor (fill factor void of series resistance losses) after application of dielectric paste B.

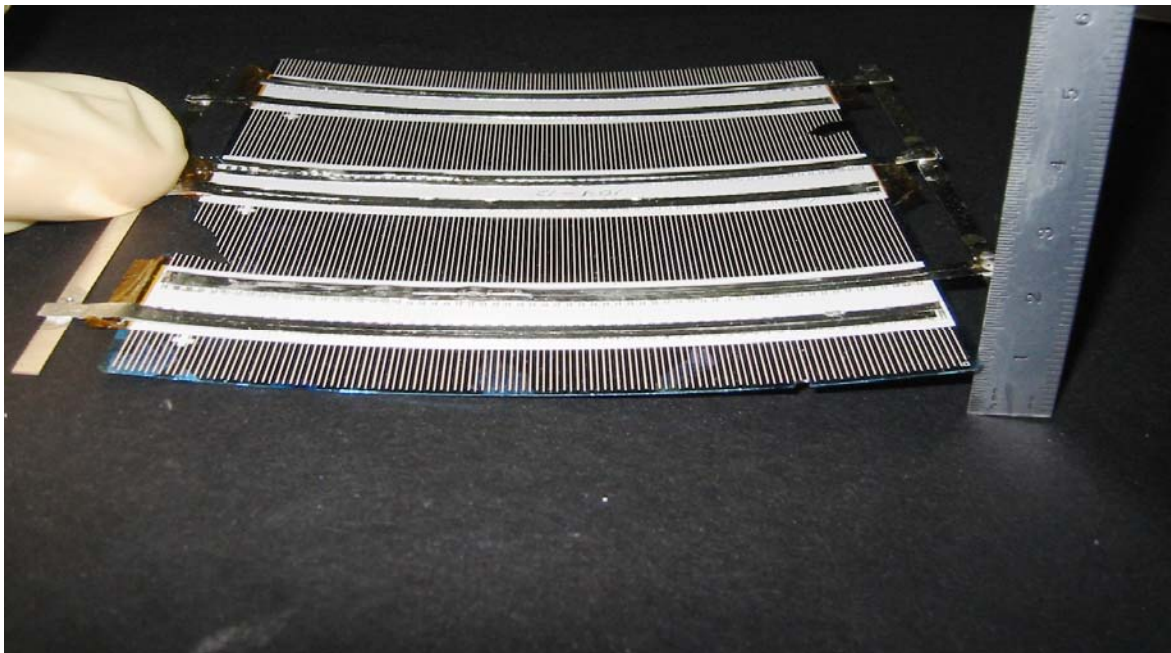


Figure 12. Bow associated with manually soldering copper ribbon conductors to the screen-printed silver gridlines. Greater than 8 mm of bow is observed when measured in the manner shown.

Conductive adhesive materials that were tried led to a significant reduction in the bow (Figure 13) because they did not require an elevated temperature to reflow or cure, so development work was carried out primarily using conductive adhesive materials rather than solder.



Figure 13. A busbarless cell using conductive adhesive to connect the screen-printed Ag gridlines to the copper ribbon. It exhibits negligible bow compared to a cell with the soldered copper ribbon.

Research Method to Isolate Screen-Printed Busbars and High Series Resistance Areas of the Cell

We examined two ways to physically isolate the active area of the cell from the screen-printed busbars: laser scribing and dicing saw. Either method has the potential to damage the n+/p junction that exists on both sides of the EWT cell. In fact, both the laser and the dicing saw affected the cell properties. The non-ideal diode saturation current (J_02) measured by the Suns-Voc technique increased after placing the dielectric on the cell rear, and increased more after using the dicing saw to remove the busbars to make busbarless EWT proof-of-concept cells. This increase is shown in Figures 14 and 15 for two different experiments below.

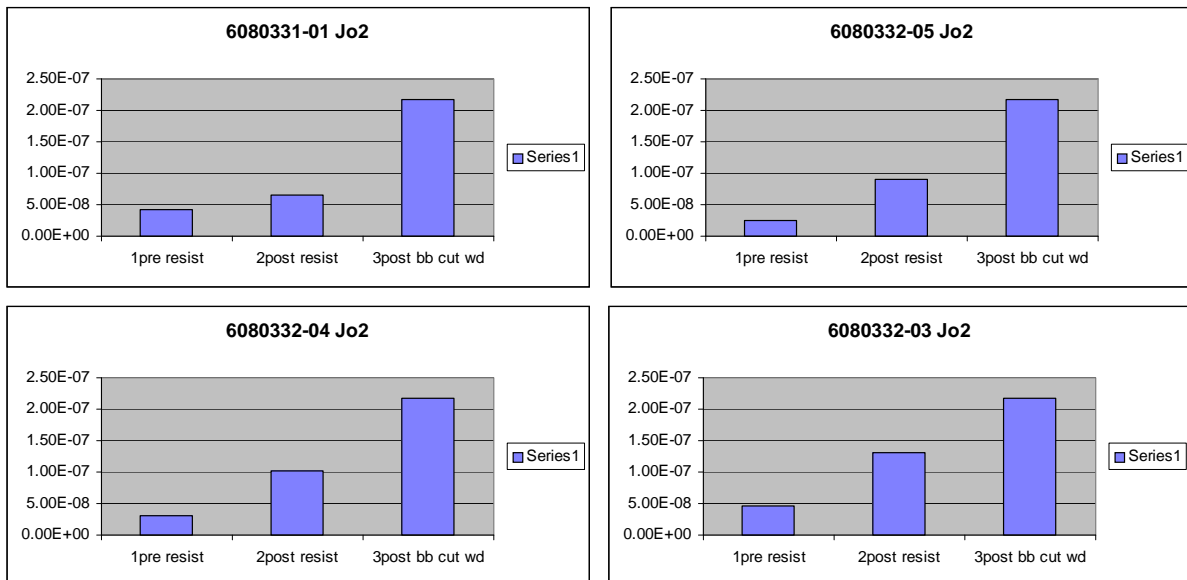


Figure 14. Demonstration of the increase in the non-ideal diode saturation current J_02 that occurs as the dielectric resist is applied and after the busbars are cut with the dicing saw ("wd" in figure axes). The increase in J_02 leads to a decrease in the fill factor.

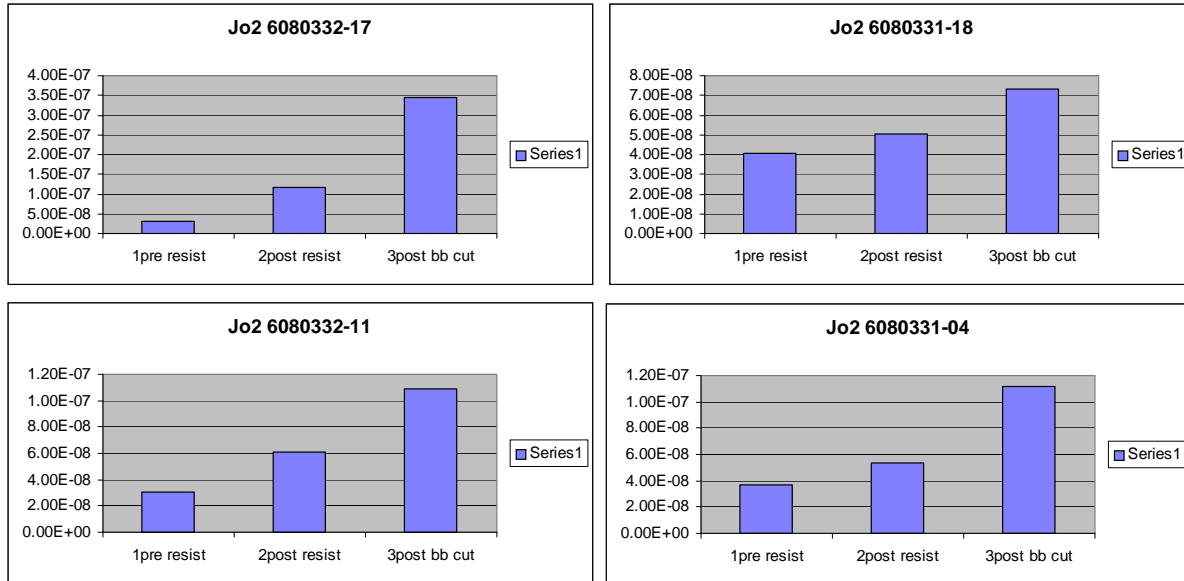


Figure 15. Demonstration of the increase in the non-ideal diode saturation current Jo_2 that occurs as the dielectric is applied and after the busbars are cut with the laser (“bb cut” in figure axes). The increase in Jo_2 leads to a decrease in the fill factor.

Fabricate and Test Proof-of-Concept Cells

Proof-of-concept cells were made in the following stages:

1. Obtain existing 125 mm × 125 mm baseline EWT cells and their cell test information from the pilot line.
2. Screen-print dielectric material to create vias for the contacts between the gridlines and the connecting ribbon and to isolate the gridlines of opposite polarity.
3. Cut off screen-printed busbars.
4. Screen-print or manually apply solder paste or other conductor at the vias for the contacts between the gridlines and the connecting ribbon.
5. Manually connect wire ribbons to each gridline—three ribbons for each polarity.
6. Test the modified cell.

The sequence to produce such cells is illustrated in Figures 16 through 19.

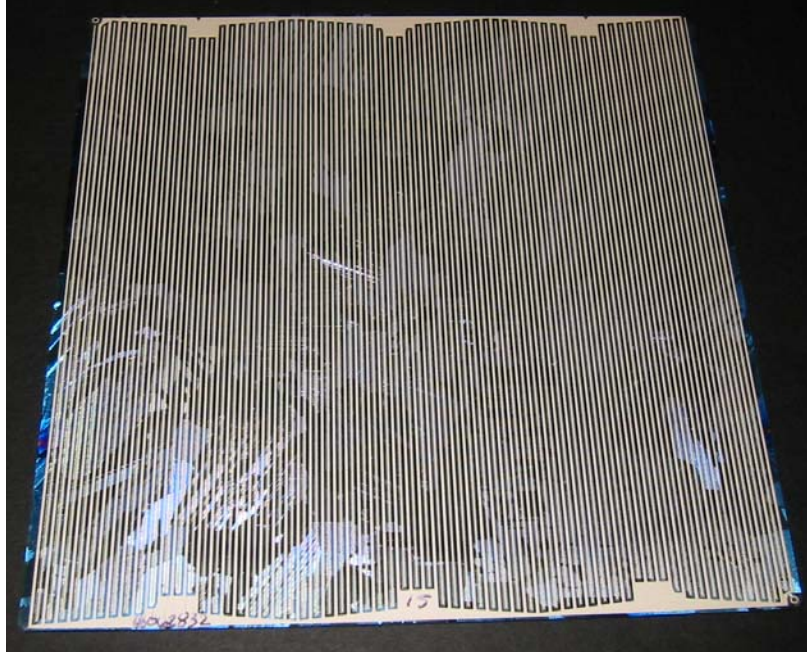


Figure 16. Baseline cell at Stage 1 – with screen-printed and sintered Ag busbars and tabbing areas located at opposite extremities of the cell.

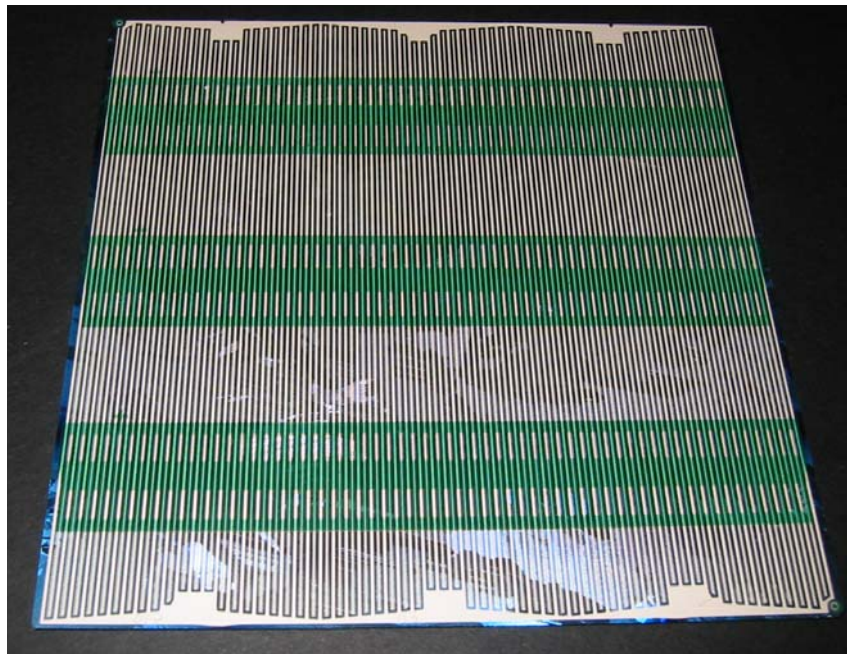


Figure 17. Stage 2 – the screen-print dielectric material is applied to create vias for the contacts between the gridlines and the connecting ribbon, and to isolate the gridlines of opposite polarity.

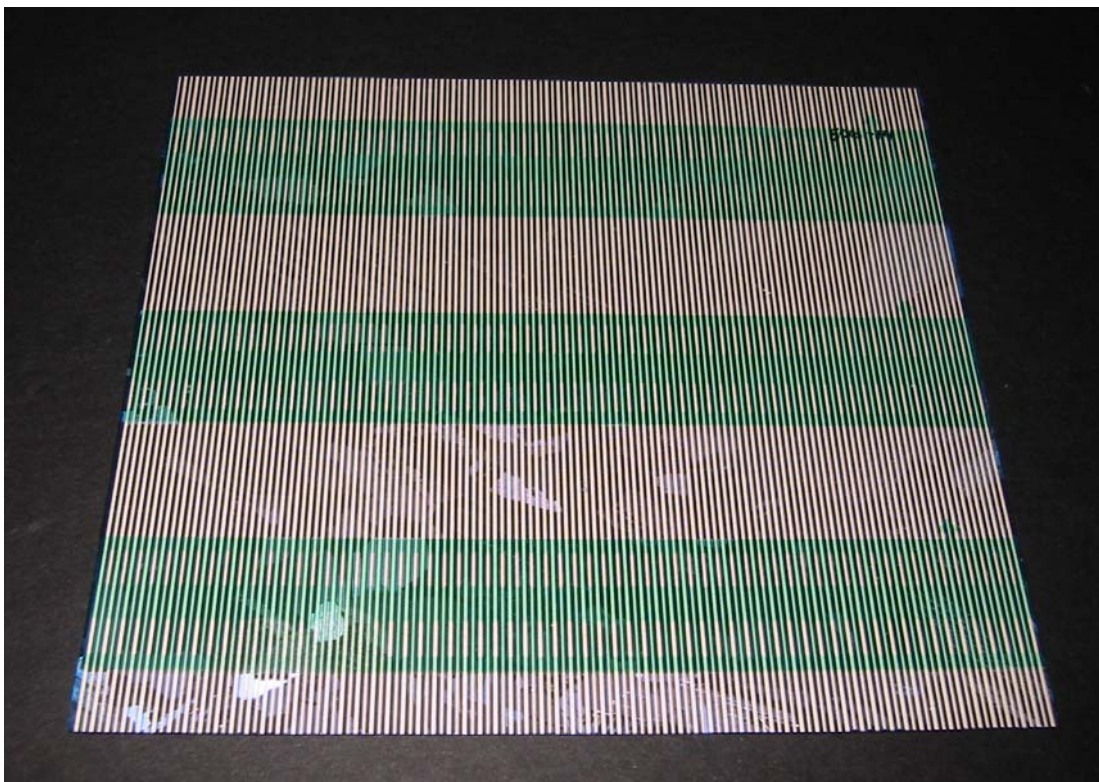


Figure 18. Screen-printed busbars are cut off with laser or dicing saw.

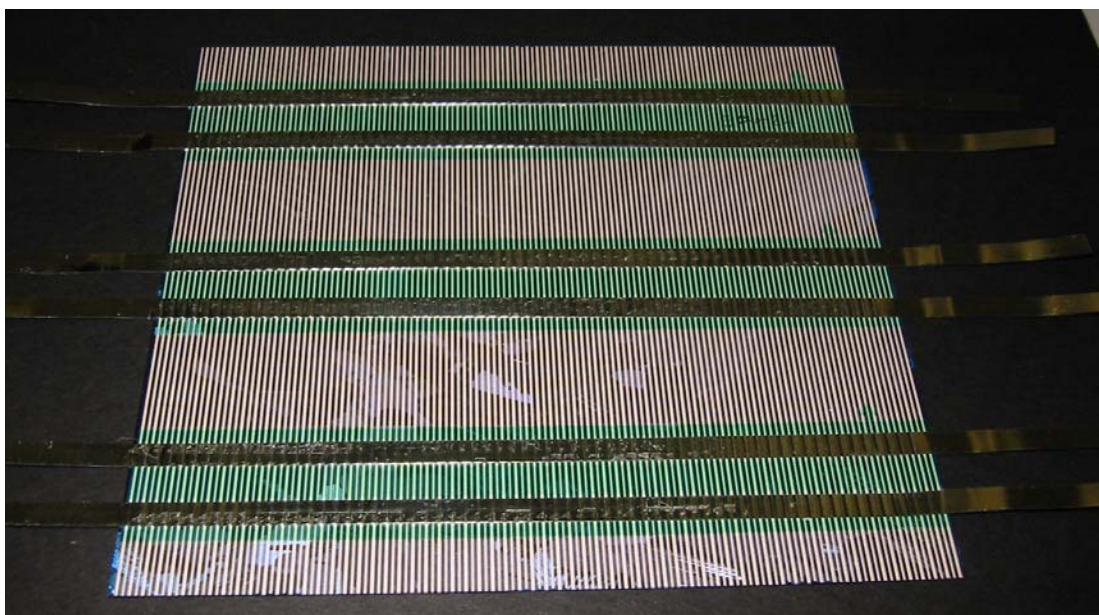


Figure 19. Wire ribbons are manually connected to each gridline with conductive adhesive – three copper ribbons are used for each polarity.

We examined cell results before and after the conversion of baseline cells to busbarless EWT cells. Results for two cells are given in Table 1.

Table 1. Cell test results measured for the EWT cell before the start of the busbarless conversion, measured after printing of the dielectric and application of the copper ribbons, and measured after laser cutting of the busbars.

Cell ID	LOT	Notes	Isc (A)	Jsc (A/cm ²)	Voc (V)	Fill Factor	Efficiency %
1	TST-6030318-01	baseline	5.325	0.0341	0.5832	68.67	13.65
1	6030318-01	ribbon tabbed busbar intact	5.41	0.0346	0.585	70	14.1
1	6030318-01	laser cut busbar	4.85	0.0348	0.583	69	14
30	TST-6030701-25	thin print baseline	5.442	0.0348	0.5808	59.76	12.09
30	6030701-25	ribbon tabbed busbar intact	5.54	0.0355	0.586	67	14
30	6030701-25	laser cut busbar	4.98	0.0355	0.584	68	14.1

Table 1 indicates that the fill factor is improved significantly when the current no longer needs to be transported across the cell length to the bonding pads at the cell edge. The copper ribbons distributed at three locations per polarity significantly reduces the power losses because power losses increase as the square of the length of the current carrying gridline. After cutting off the busbars to remove the edge diode series resistance, the fill factor did not noticeably improve. This may be explained, at least in part, by the degradation in the cell junction properties (J_0 , the non-ideal diode saturation current) associated with the cell cutting discussed in Figures 14 and 15.

Achieving a Prototype 15% Busbarless Cell

Because of the losses in the non-ideal diode saturation current (J_0) associated with the cell cutting procedure shown in Figures 14 and 15 and efficiencies short of our goal of 15% in Table 1, we decided to fabricate the prototype cells that do not require busbar removal by cutting. For the prototype cell development, we determined a suitable pattern for the emitter wrap-through micro through-holes, geometries of the device, dielectric, metallization, ribbons, and interconnects.

We processed Si wafers with the prototype 125 mm × 125 mm cell design. The process steps are laser drilling, saw and laser damage removal by etching, application and verification of diffusion barrier material, diffusion, application of silicon nitride, screen-printing of positive and negative gridline contacts, screen-printing of dielectric material, and application of conductive adhesive and copper ribbon bussing material. A completed prototype cell is shown in Figure 20.

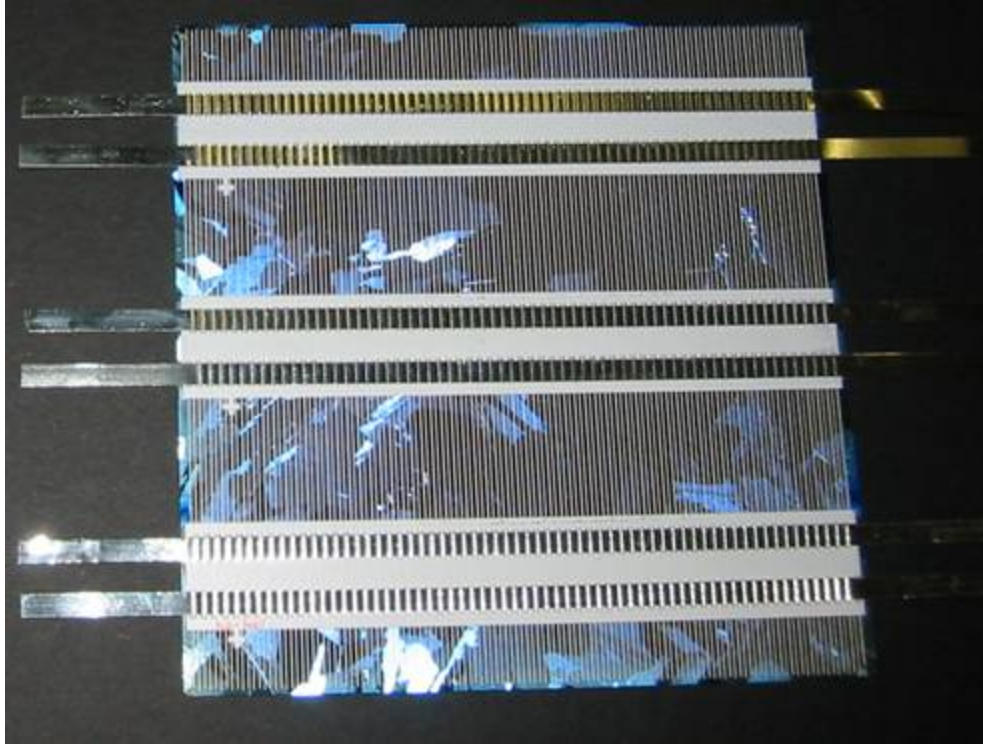


Figure 20. Complete 125 mm × 125 mm prototype cell.

Several functional prototype cells were completed. The best cell had a measured conversion efficiency of 15% as detailed in Table 2.

Table 2. Efficiency measurement of three prototype busbarless cells.

Cell ID	Fill Factor	Efill Factor %	Voc	Isc	Jsc (mA/cm²)	Pmp
6091104-03	72	15.00	0.588	5.5	35.20	2.341
6091104-04	72	14.80	0.589	5.51	35.26	2.307
6091104-08	71	14.80	0.589	5.51	35.26	2.308

PRODUCTION OF 125 MM × 125 MM BUSBARLESS CELLS

Engineering Design of 125 mm × 125 mm Busbarless Cells

Cell Design

The initial prototype cell design described in the previous section, which was based on the Advent production cell design, was reviewed and modified to arrive at the busbarless cell design described herein. The initial prototype cell had a dielectric layer applied over the existing gridlines as can be seen in Figure 21. The gridlines in this cell are tapered from one end of the cell to the other and terminate in the bond pads at each end. The design of the true busbarless cell eliminated the bond pads at the edge of the cell, eliminated the taper of the gridlines while maintaining the same pitch and incorporating small bonding pads at intervals along each gridline as can be seen in Figure 22.

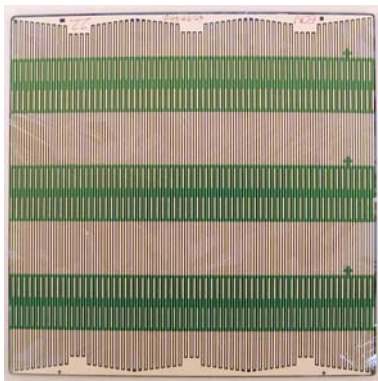


Figure 21. Prototype busbarless cell with dielectric printed.

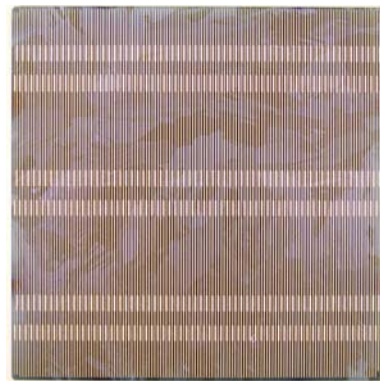


Figure 22. Busbarless cell before dielectric print showing three rows of bussing pads for each polarity.

The width of the p and n metal gridlines was made 300 μm . This allowed the height of the metal traces to be reduced while maintaining the cross-sectional area. Maintaining the cross-sectional area is expected to reduce the contact resistance without impacting the resistivity of the gridlines or requiring additional Ag. An added enhancement of this design change was to further reduce the bow in the cell due to paste height having slightly more impact on bowing than paste width.

The width of the dielectric overlay was increased to provide more protection against adhesive overrun. Initial work with conductive adhesives was hampered by pushout from under the ribbon. Increasing the width of the dielectric provided more tolerance for the overrun of the adhesive. The length of the dielectric print was also modified to extend over the edge of the cell. This was done in response to several cells that exhibited shunting at the edge of the cell near the last p bond pad. The final design is shown in Figure 23.

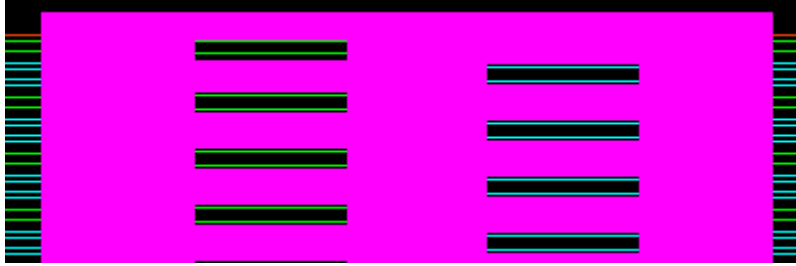


Figure 23. Revised dielectric shown over p and n metal traces.

Development of Cell Measurement Techniques

Several probing designs were investigated to measure the current voltage (IV) and other electrical characteristics of cells that did and did not have dielectric printed on the cell. The purpose was to provide a means by which an un-bussed cell could be tested and the effects of dielectric printing and bussing could be quantified. Also, it was desired to be able to measure the final assembled busbarless cell performance that has bussing ribbon attached to the cell using test lead wires.

The probe configurations were designed to fit into a single jig (Figure 24) that provided alignment to both 125 mm × 125 mm and 156 mm × 156 mm cells with the use of an insert. The frame of the jig allows one or more probe bars to be added, providing a wide variety of probing configurations.

Two approaches were investigated – pogo pins and copper balls. The pogo probing bar consisted of four parallel rows of narrow pogo pins with two pins contacting each bussing pad. This probing configuration was Kelvin and eliminated the contribution of contact resistance (Figure 25).

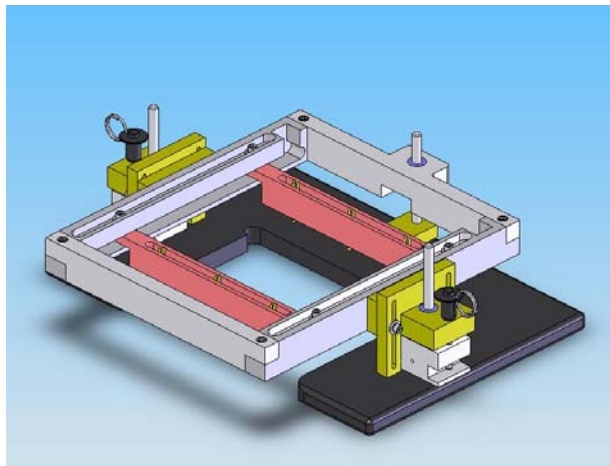


Figure 24. Solid works rendering of jig with two probe bars in place.

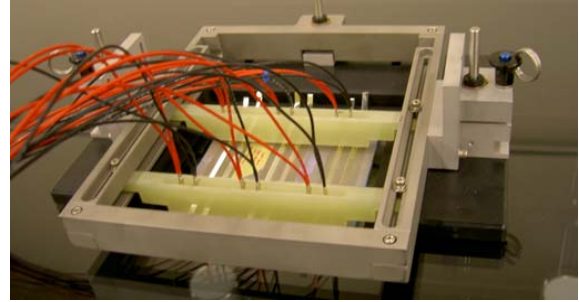
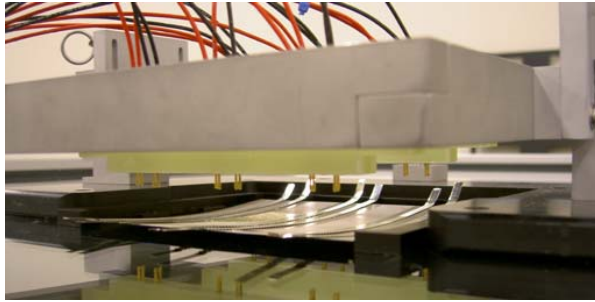


Figure 25. The probe jig is shown configured to measure a bused cell. The configuration of the pins is such that the probing system is Kelvin.

The ball bearing or copper ball probing jig shows a design that we made to make contact to every gridline (Figures 26 through 28). Tests indicated that the jig was able to make contact to the gridlines while not requiring a great deal of down force.

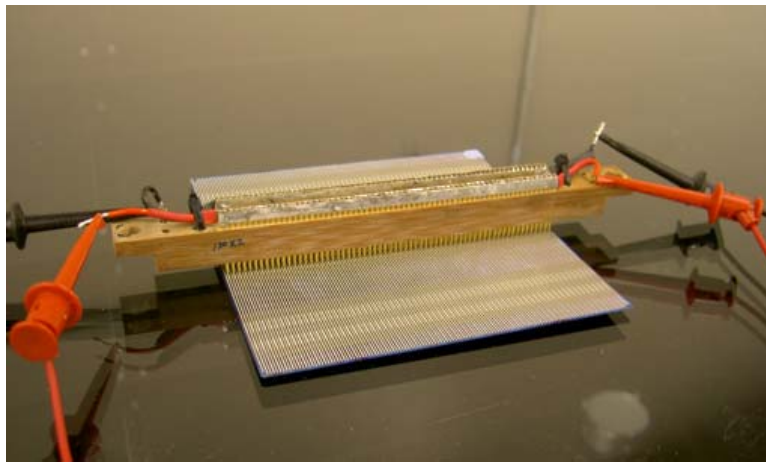


Figure 26. Pogo probe bar with test leads attached.

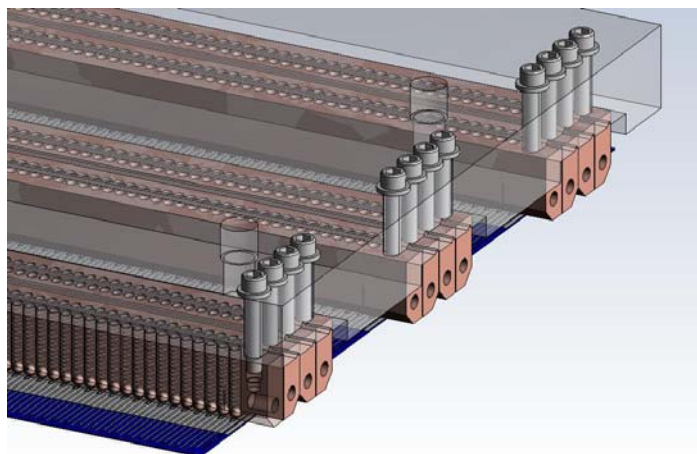


Figure 27. Solid works drawing showing assembled copper ball jig on a cell.

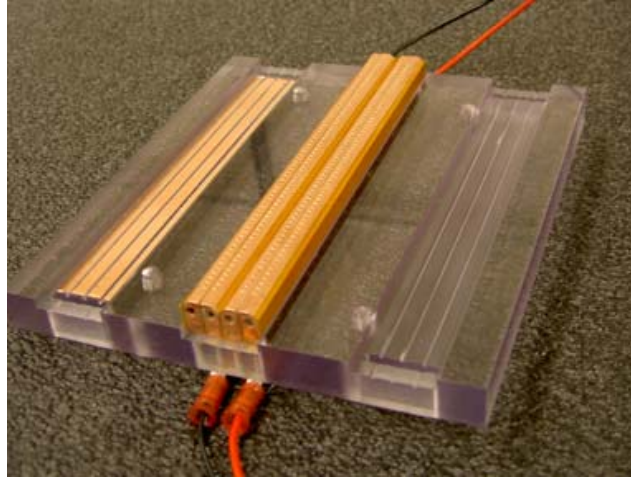


Figure 28. Copper ball test jig with center bars assembled.

The following graphs (Figure 29) summarize the fill factor and cell efficiency of 10 cells measured with the ball bearing jig.

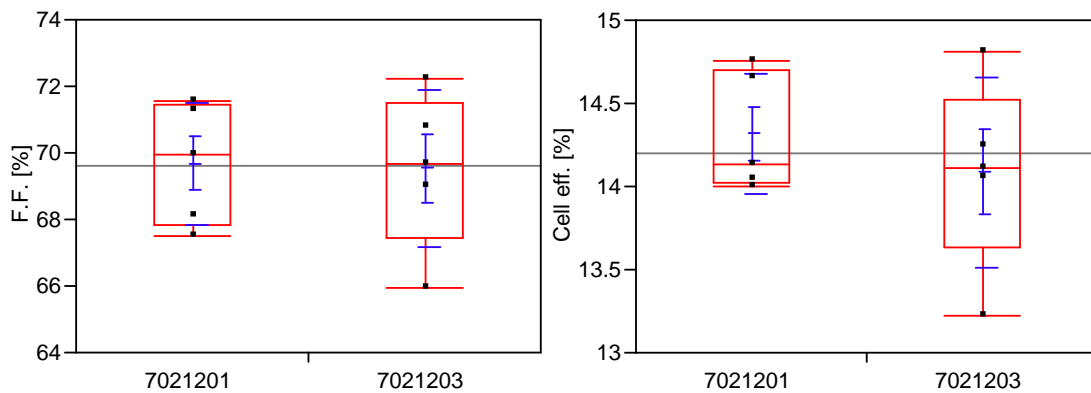


Figure 29. Fill factor and cell efficiency of ball bearing EWT (BBEWT) cells measured with the copper ball bearing jig, for two different lots, as labeled.

Stress Modeling

Due to the differing temperature coefficients of expansion (TCEs) of copper and Si, solder bond failure is the most common failure mechanism for solar modules. The unique design of the busbarless EWT cells amplifies this problem as it requires a bus contacting many points across the entire cell length. Conductive adhesives and low-temperature solders are options for reducing stresses. Preliminary analysis has been performed assuming the bus can be cured/soldered at 150 °C.

One approach is to use beam flexure formulas and model the assembly as a compound beam. Modeling predicts that curing the bus at 150 °C and cooling to 25 °C will result in an edge lift of 32.3 mm. Edge lift is the height of one wafer edge if the opposite edge is held against a flat surface. Actual measured samples ranged from 14 mm to 22 mm of edge lift.

A model was also created using COSMOS FEA software in an attempt to better understand bowing issues observed after bussing and allow theoretical solutions such as compliant busses to be tested before fabrication. The deformation predicted is approximately 2x the actual measured deformation.

Both approaches predicted greater deformation than found in laboratory experiments, and the predicted stress of the COSMOS analysis should be enough to shear the adhesive bond line. Shearing was not found to occur during experimental bussing. Several aspects not reflected in the models may account for these discrepancies. The material properties for pure Si and pure copper were used, neglecting the impact of solder coating on the ribbon, the multicrystalline nature of the wafers, and the various layers created in cell processing (Si_3N_4 , diffusion barrier, metal gridlines). The bond pads were modeled as mesas on the wafer and do not reflect any plastic deformation that may be occurring at the bond line.

One of the most likely contributing factors is that the experimental cells were all bussed with ribbed ribbon. Early experiments with soldering had shown the ribbon to relieve some of the mechanical strain. Actual test data is needed to further refine the model; various values have been reported for the mechanical properties of multicrystalline Si depending on the wafer manufacture process or test source, and may not be applicable to Advent's wafers. In addition, the mechanical effects of Advent's unique laser drilling process have not yet been fully captured.

Pull testing of cells bussed with various conductive adhesives exhibited pull strength between 0.5 Newton and 7 Newton. A reasonably successful curing regime gave pull strength results in the 3 Newton range as shown in Figure 30. Tests with various conductive adhesive materials are given in Table 3.

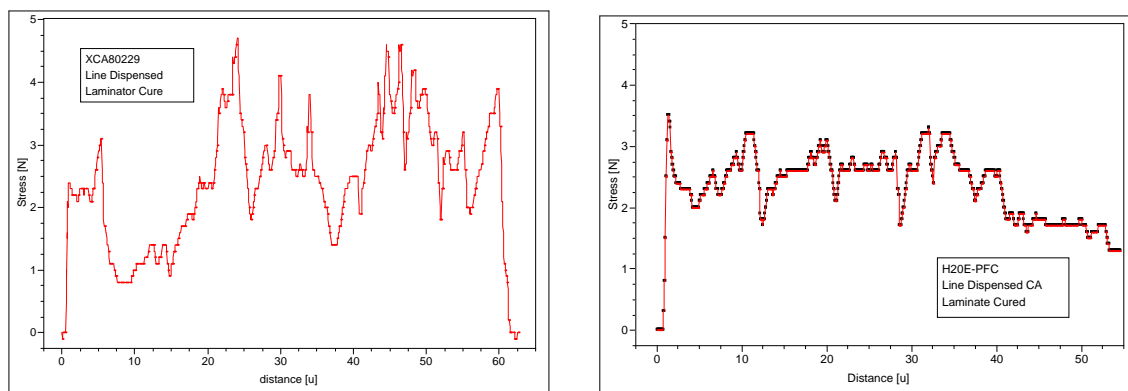


Figure 30. Comparison of pull strength of cells bussed with adhesive 3 (left) and adhesive 1 (right).

Table 3. Pull tests with various conductive adhesive materials.

Adhesive	Peak Force (N)	Avg. Force (N)
Adhesive 1	2.10	0.46
Adhesive 1	0.50	0.03
Adhesive 1	1.60	1.07
Adhesive 2	5.40	2.20
Adhesive 2	3.10	1.14
Adhesive 2	2.60	1.40
Adhesive 3	4.70	2.41
Adhesive 4	1.80	0.45
Adhesive 4	1.70	0.84

Single-Cell Accelerated Testing

Four cells were laminated with acrylic tape placed on the back of the cell to determine if the tape could be used as a dielectric material. After 300 thermal cycles the tape did not exhibit any signs of physical degradation, bubbling, or delamination from the back of the cells. A typical cell is shown in Figure 31. The IV results of the cell performance before and after testing are shown in Figure 32. The increase in short circuit current (I_{sc}) and maximum power current (I_{mp}) is most likely due to simulator calibration error. The results indicated that the material may make a promising candidate for a tape-based dielectric.

Four cells with blue pigmented dielectric were printed on modified Carlsbad cells and subjected to 300 thermal cycles. The cell shown in Figure 33 exhibited excellent durability. The efficiency of the cells remained stable within 4% of the original measured power. The I_{sc} and I_{mp} changes are likely due to calibration issues of the solar simulator. The IV characteristics for all the cells are summarized in Figure 34. We also observed that there was no visual degradation of the cell. The dielectric showed no signs of delamination.

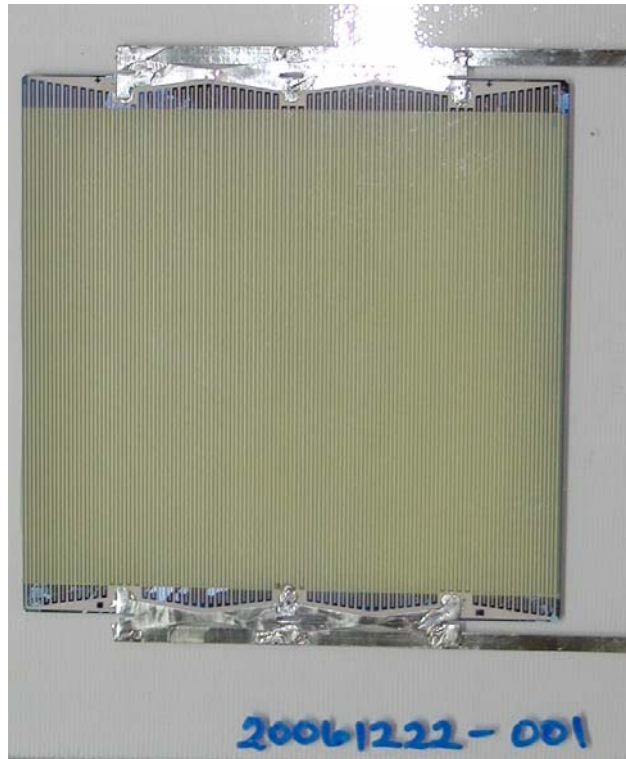


Figure 31. Carlsbad cell tested in thermal cycle to access the effect of dielectric tape on cell performance.

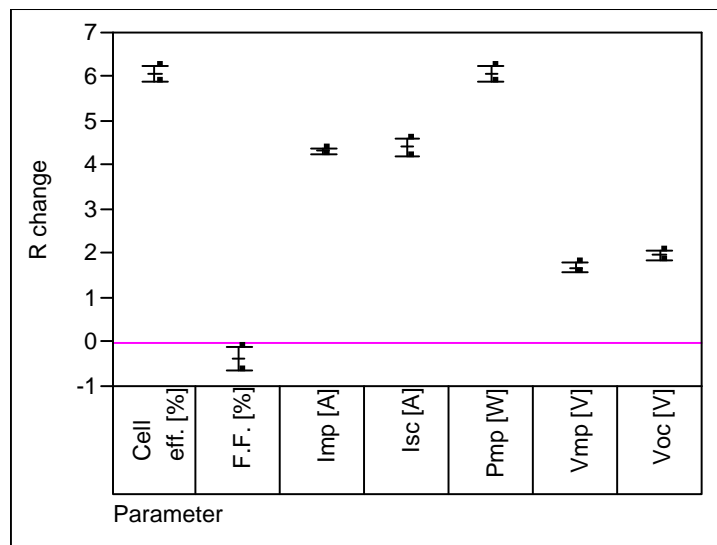


Figure 32. Summary of tape dielectric effect on cell performance after 300 thermal cycles. The relative change R (%) is indicated.

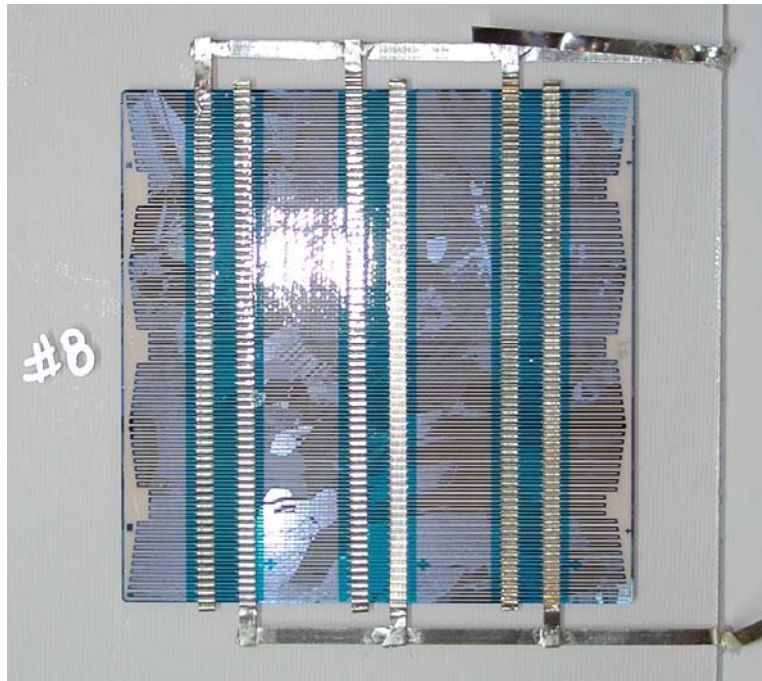


Figure 33. Modified Carlsbad cell after 300 thermal cycles.

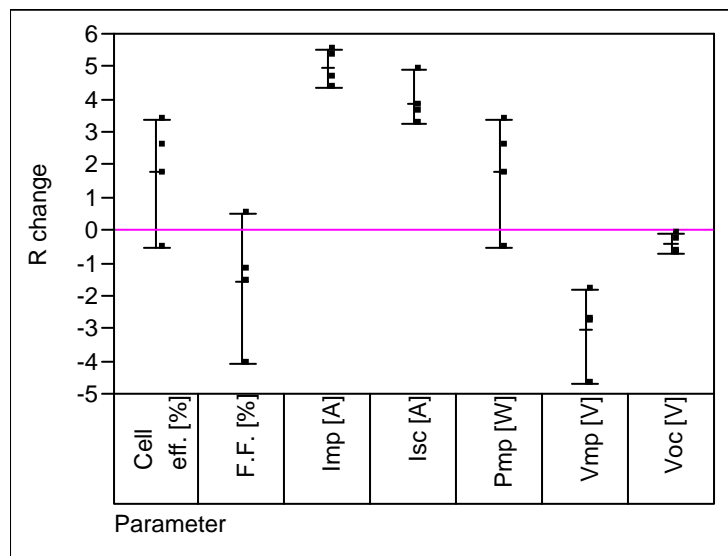


Figure 34. Summary of modified Carlsbad BBEWT cells subjected to 300 thermal cycles. The relative change R (%) is indicated.

PRODUCTION OF EWT CELL MINI-MODULES AND TEST

The technical challenge now faced is how to assemble busbarless cells into modules with a production scalable process. Before investing in an automated module assembly system, we first sought to hand-assemble proof-of-concept modules for accelerated testing.

String and Encapsulate 12-Cell and Other Multi-Cell Laminates

Review of Bus Requirements and Candidates

A mathematical model was developed to determine minimum cross sectional bus areas based on work by Meier and Schroder.⁴ An R_s maximum of $0.0610\Omega\text{-cm}^2$ was determined based on an acceptable module power loss. Each of the conductor candidates was then rated accordingly. Although the current project is utilizing $125\text{ mm} \times 125\text{ mm}$ cells, the calculations are based on a $156\text{ mm} \times 156\text{ mm}$ in preparation for target production size.

Several different geometries of copper bus interconnect were investigated. The main drivers were stress relief, cost, and implementation. Because of the large cross-sectional interconnect area combined with the requirement that it be bonded to every other gridline, alleviation of stress due to thermal expansion presents a major design challenge.

Pull Tests of Interconnects

To characterize the stress-relieving nature of the ribbons, they were cut to widths providing total cross-sectional areas equivalent to the $4\text{ mm} \times 0.2\text{ mm}$ ribbon and placed in a pull tester. The results are indicated in Figure 35.

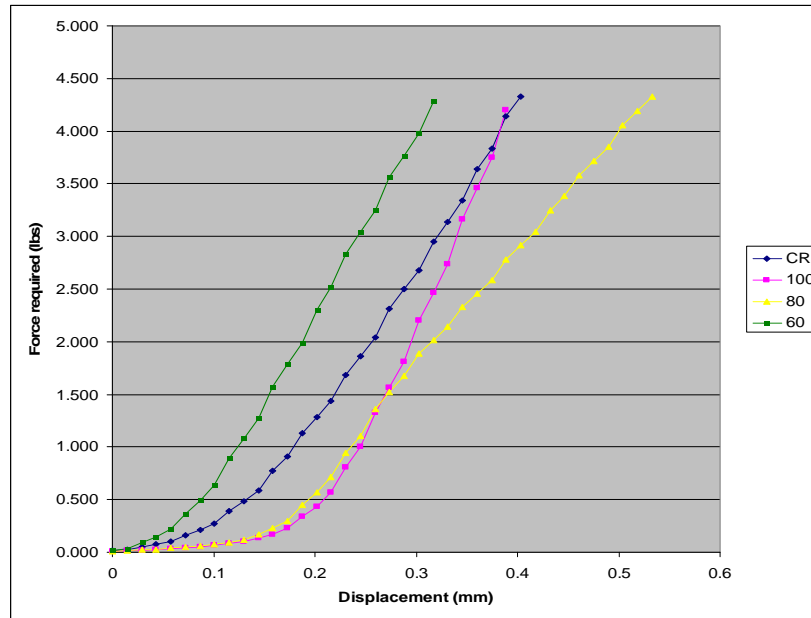


Figure 35. Results of pull test indicating pull force vs. displacement for various interconnects

⁴ D. L. Meier and D. K. Schroder, *IEEE Transactions on Electron Devices*, Vol. ED-31, No. 5, May 1984, pp. 647-53.

String Fabrication

Individual cells were bussed in strings of three with the middle cell inverted to connect the alternating polarities with straight bus segments (Figure 36).

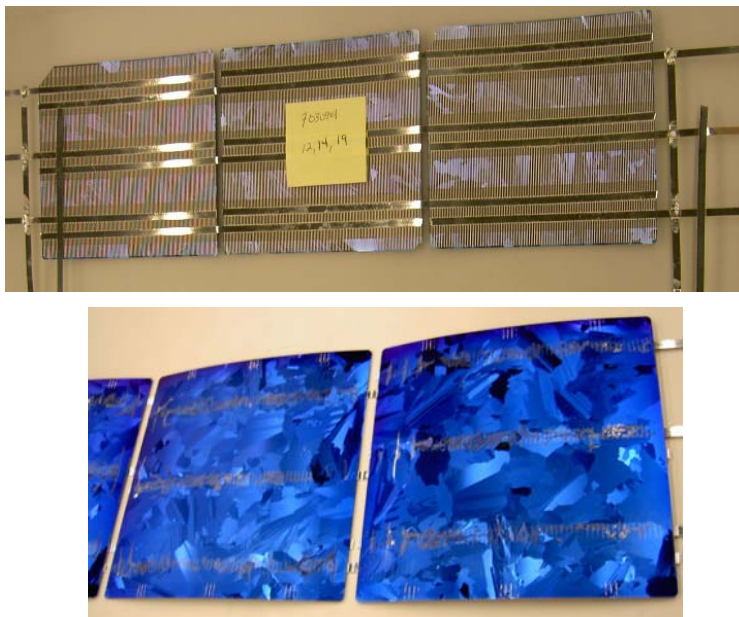


Figure 36. Busbarless cell strings shown interconnected with wire cloth. Rear is shown on top images and the light facing side is shown on the bottom. Conductive adhesive bleed-through can be seen on the cell face at this stage of the process, but it is not discernable after encapsulation.

As a result of the alignment requirements, each three-cell string required 15 to 30 minutes of assembly time. The completed strings were then measured on the Quick Sun Module tester against a 3×4 cell module of Advent's standard back contact 125 mm cells that was calibrated at Sandia National Laboratories. Some front side discoloration resulted from adhesive bleed-through during the curing process; however, this bleed-through could not be discerned after encapsulation.

MODULE FABRICATION

The strings were then matched together based on Isc and bussed into a single unit using 4 mm × 0.2 mm ribbon with 96.2 Sn/0.3 Ag leadless solder. Test modules with the configurations listed below were assembled with Advent Solar's standard module materials in a vacuum press lamination process.

- One 3 × 4 module with conductive adhesive and ribbon (Figure 37)
- One 3 × 3 module with conductive adhesive and ribbon
- One 3 × 3 module with conductive adhesive and ribbon
- One 1 × 3 string conductive adhesive and ribbon
- One 1 × 3 string conductive adhesive and ribbon

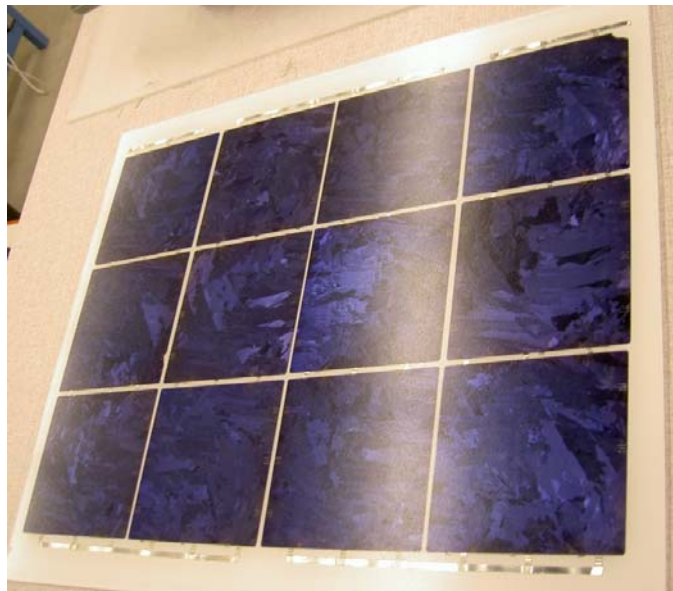


Figure 37. A 12-cell busbarless module.

After assembly, the modules were tested against a 3 × 4 cell module of Advent's standard 125 mm × 125 mm EWT cells that was calibrated at Sandia National Laboratories. The 3 × 4 busbarless module, which incorporated the best performing strings built with ribbon and conductive adhesive, produced 27.3 watts of power with a 0.74 fill factor. For comparison, the calibration module is rated at 26.5 watts with a fill factor of 0.68 (room temperature conditions) – typical for conventionally interconnected EWT modules.

One notable result was evidence that our ball bearing test probe (used to test cells before bussing) was proven to be less than adequate. As seen in Figure 38, mapping of the individual cell measurements shows lower fill factors than the completed strings or module. Testing the completed string and module is the more straightforward measurement compared to the ball bearing tester because of the 774 contacts the ball bearing test probe must make.

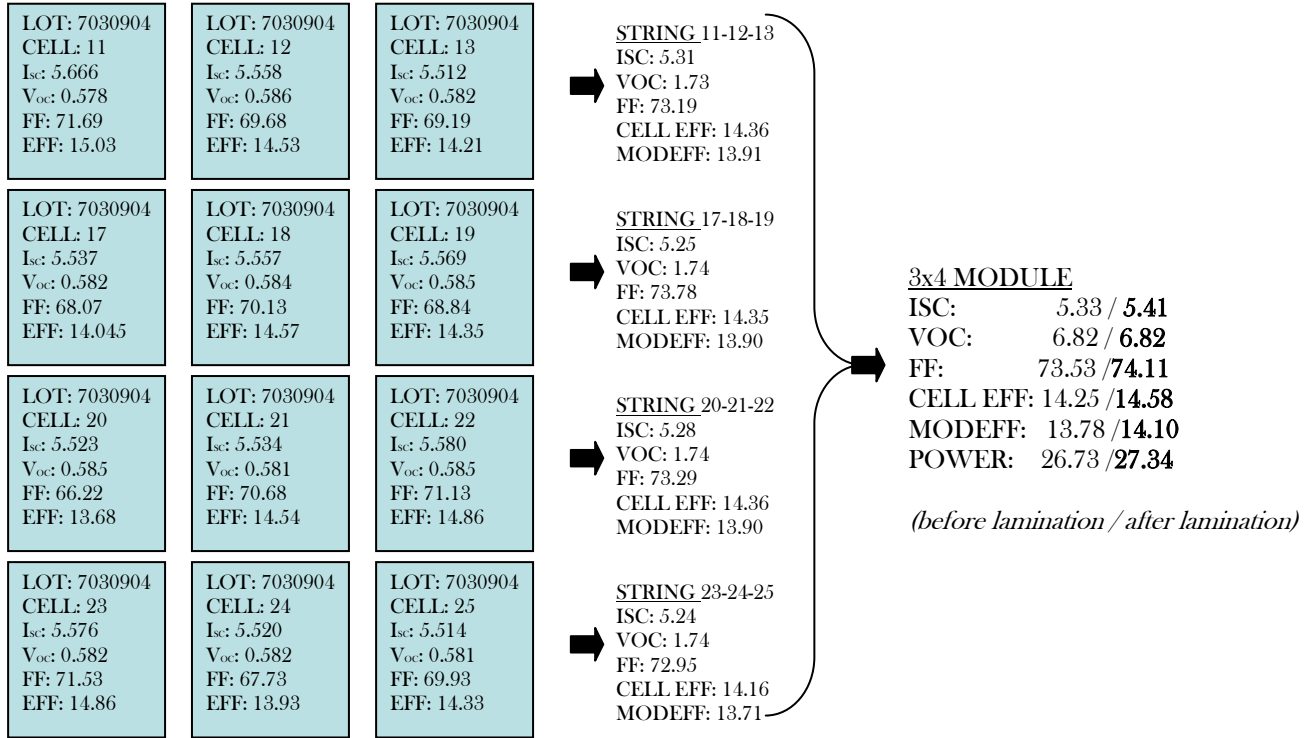


Figure 38. Component cell performance parameters as measured by the ball bearing cell tester; string, module (before and after lamination) performance parameters measured with a QuickSun module tester.

Summary of Busbarless Mini-Module Test Results

Twelve-, nine-, six- and three-cell busbarless cell mini-modules were produced by manual assembly. Conversion efficiencies of the mini-modules were extremely favorable due to the significantly improved fill factor as made possible by the busbarless technology (Table 4). Fill factors of the 12-cell mini-module showed the capability of exceeding 0.74 as compared to the 0.69 or 0.70 best values achieved for the conventional edge-tabbed EWT cell modules with screen-printed Ag metallization. A nine-cell module efficiency of 14.5% was achieved with fill factor of 0.734.

Table 4. Module test results for six minimodules produced with busbarless cells.

Lot-module: cell array, interconnect/ conductive adhesive type	# of Cycles	Time	Voc	Isc	Vmp	Imp	Pmp	Fill Factor	CellEff	Module Eff
Calibration 3x4		13-Aug-07	7.043	5.407	5.225	4.774	24.945	65.513	13.304	12.863
08132007-01: 3x4, Ribbon,	Initial	15-Aug-07	6.818	5.412	5.493	4.978	27.345	74.112	14.584	14.100
08132007-02: 3x3, Ribbon,	Initial	13-Aug-07	5.245	5.451	4.195	5.002	20.982	73.395	14.920	14.454
08172007-04: 3x3, Ribbon,	Initial	17-Aug-07	5.355	5.568	4.271	4.998	21.345	71.588	15.179	14.704
7051608-4-8-18: 1x3, Ribbon,	Initial	17-Aug-07	1.766	5.529	1.411	4.929	6.956	71.235	14.839	14.368
7051607-4-5-6: 1x3, Ribbon,	Initial	17-Aug-07	1.759	5.345	1.405	4.758	6.683	71.091	14.258	13.805

Accelerated Testing of Multi-Cell Laminates

Thermal Cycling

Thermal cycling test results for five of the successfully built mini-modules are shown in Figures 39 through 43 for 191 hours. None of the mini-modules displayed power degradation below the International Electrochemical Commission (IEC) 61215 cutoff of 5% degradation. Generally speaking, the overall power loss was not detected for three out of the five mini-modules made. These results support the use of ribbon and conductive adhesive interconnect for achieving high-reliability busbarless EWT cells.

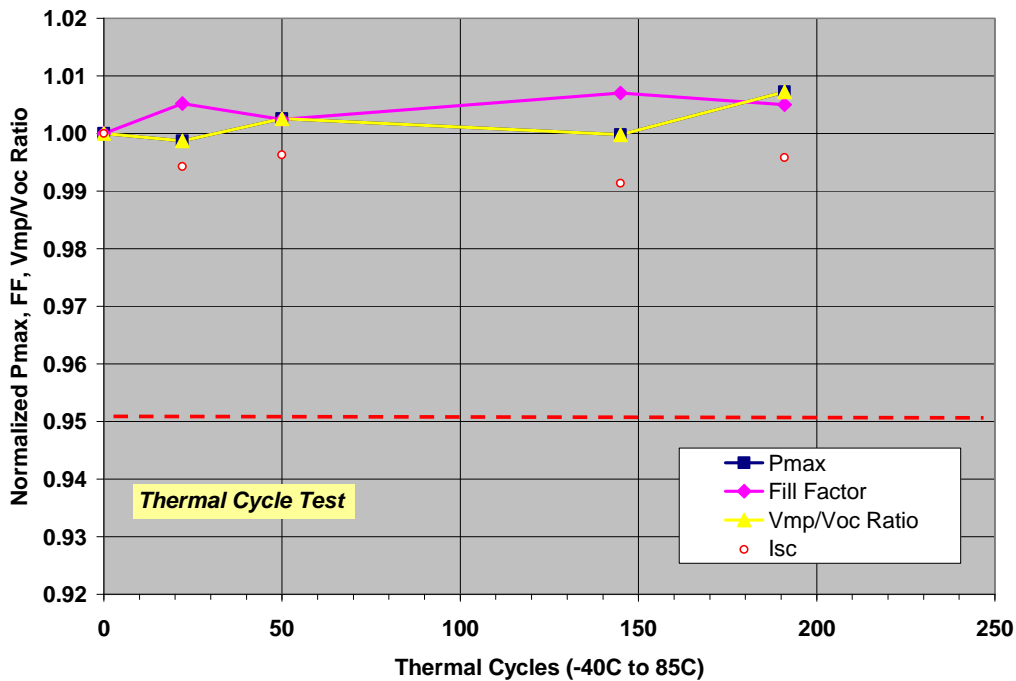


Figure 39. Results of thermal cycling tests for mini-module 08132007-01: 3 x 4 cell module with ribbon, conductive adhesive. The fraction drop in Pmax, fill factor, Vmp/Voc ratio, and Isc is shown over a period of 191 hr. This sample performed favorably in thermal cycling tests.

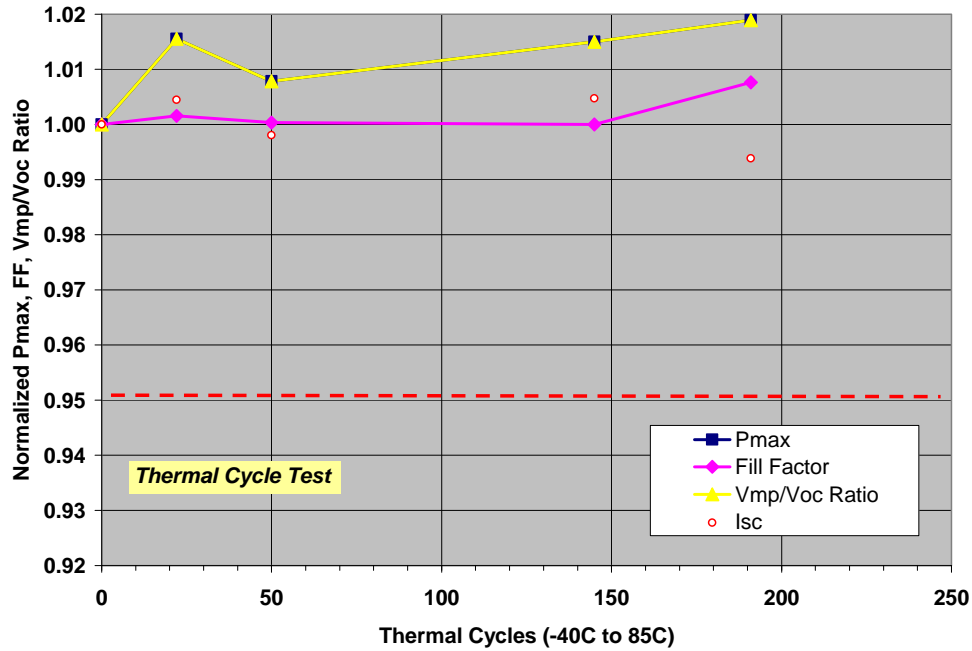


Figure 40. Results of thermal cycling tests for mini-module 08132007-02: 3x3 cell module with ribbon, conductive adhesive. The fraction drop in Pmax, fill factor, Vmp/Voc ratio, and Isc is shown over a period of 191 hr. This sample performed favorably in thermal cycling tests.

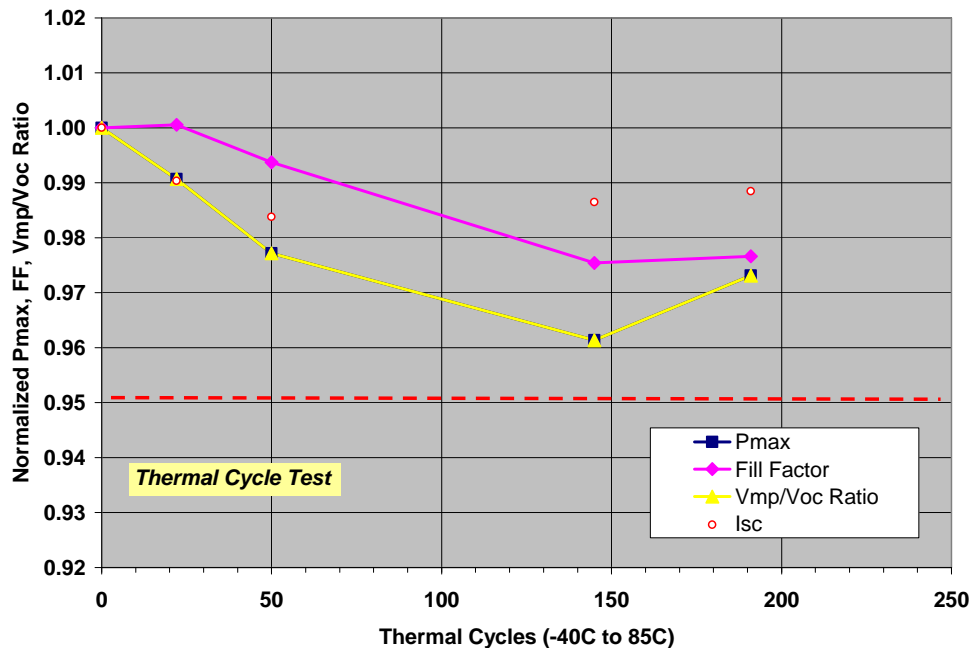


Figure 41. Results of thermal cycling tests for mini-module 08172007-04: 3x3 cell module with ribbon, conductive adhesive. The fraction drop in Pmax, fill factor, Vmp/Voc ratio, and Isc is shown over a period of 191 hr. This sample performed favorably in thermal cycling tests.

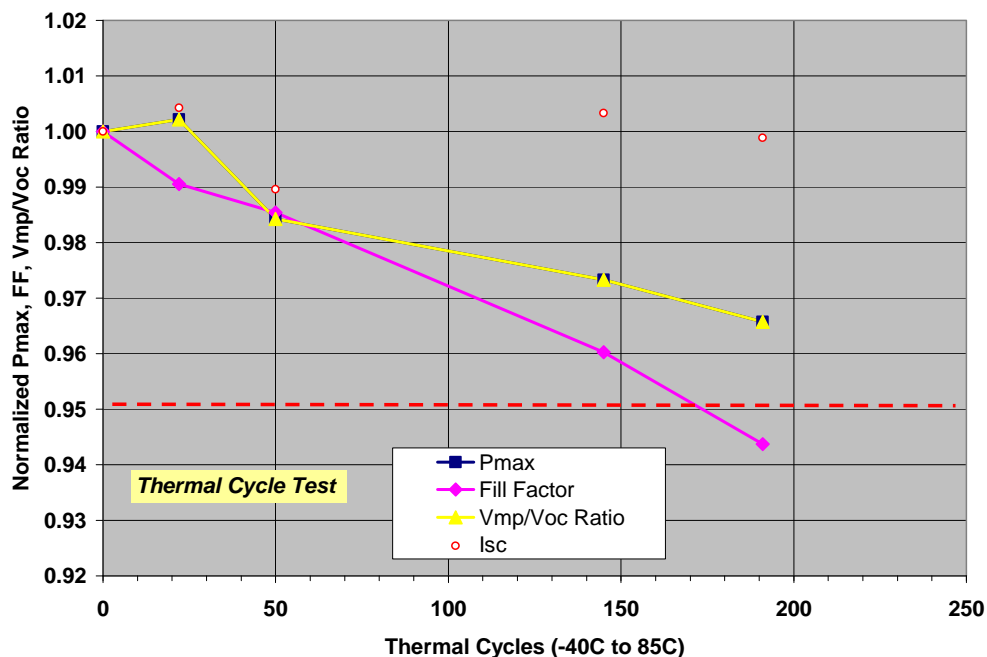


Figure 42. Results of thermal cycling tests for mini-module 7051608-4-8-18: 1x3 cell module with corrugate ribbon, conductive adhesive. The fraction drop in Pmax, fill factor, Vmp/Voc ratio, and Isc is shown over a period of 191 hr. This sample performed favorably in thermal cycling tests, although fill factor was degraded more than 5%.

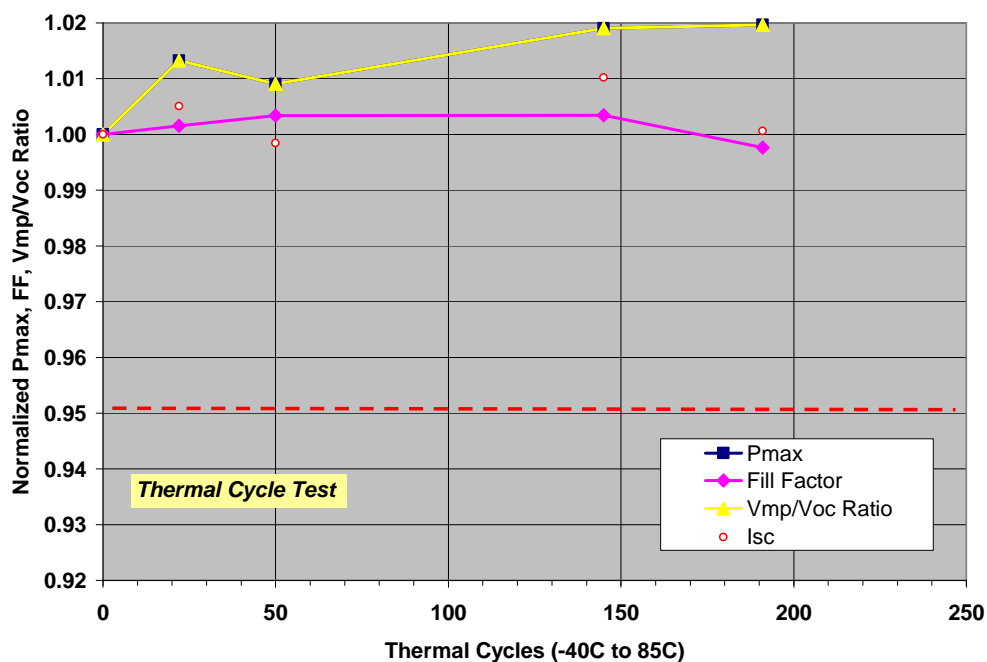


Figure 43. Results of thermal cycling tests for mini-module 7051607-4-5-6: 1x3 cell module with ribbon, conductive adhesive. The fraction drop in Pmax, fill factor, Vmp/Voc ratio, and Isc is shown over a period of 191 hr. This sample performed favorably in thermal cycling tests.

Damp Heat

Damp heat test results for five of the successfully built mini-modules are shown in Figures 44 through 48 for 1008 hours. None of the mini-modules displayed power degradation below the IEC 61215 cutoff of 5%. Generally speaking, the overall power loss was less than 2% for four out of the five mini-modules made, and mini-module 08132007-01: 3×4 cell module with ribbon, conductive adhesive displayed about 3% power loss associated with a fill factor drop. Also, these results support the use of ribbon and conductive adhesive interconnect for achieving high-reliability busbarless EWT cells.

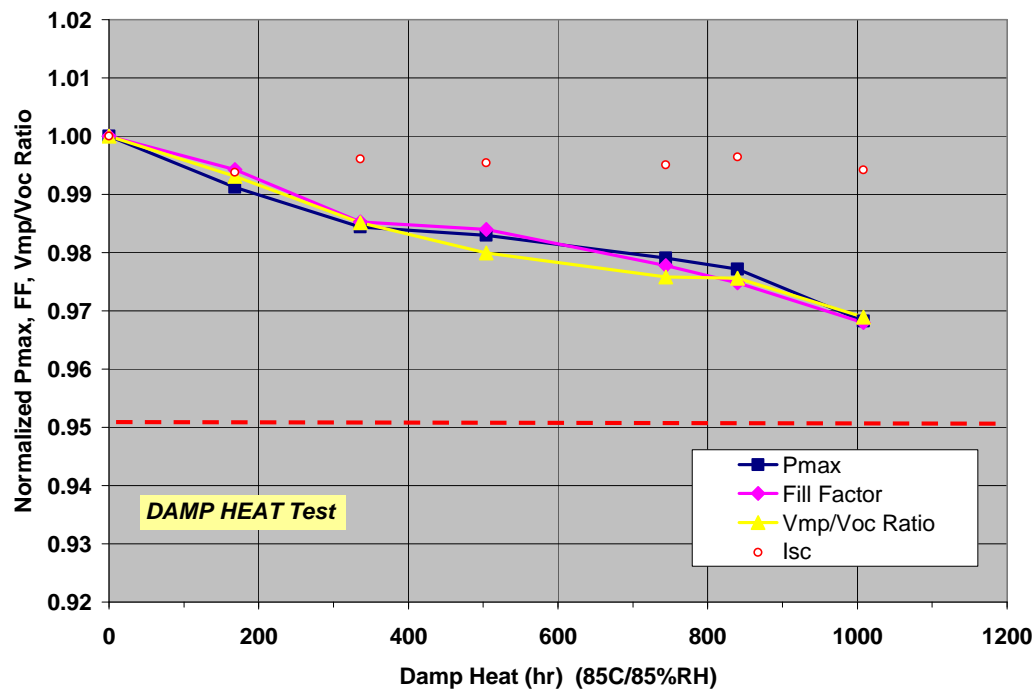


Figure 44. Results of damp heat tests for mini-module 08132007-01: 3×4 cell module with ribbon, conductive adhesive. The fraction drop in Pmax, fill factor, Vmp/Voc ratio, and Isc is shown over a period of 1008 hr. This sample performed favorably in the damp heat tests.

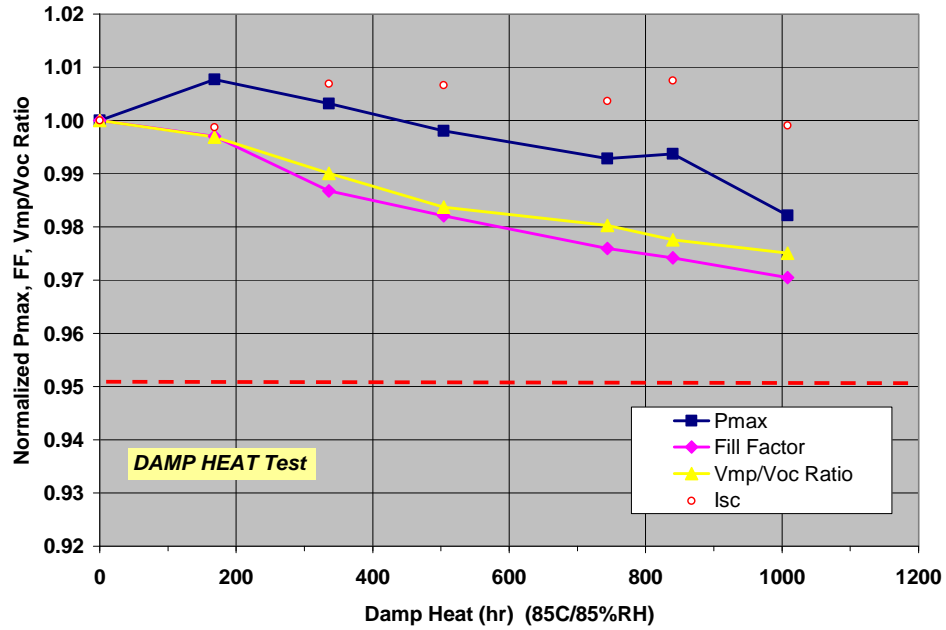


Figure 45. Results of damp heat tests for mini-module 08132007-02: 3x3 cell module with ribbon, conductive adhesive. The fraction drop in Pmax, Fill factor, Vmp/Voc ratio, and Isc is shown over a period of 1008 hr. This sample performed favorably in the damp heat tests.

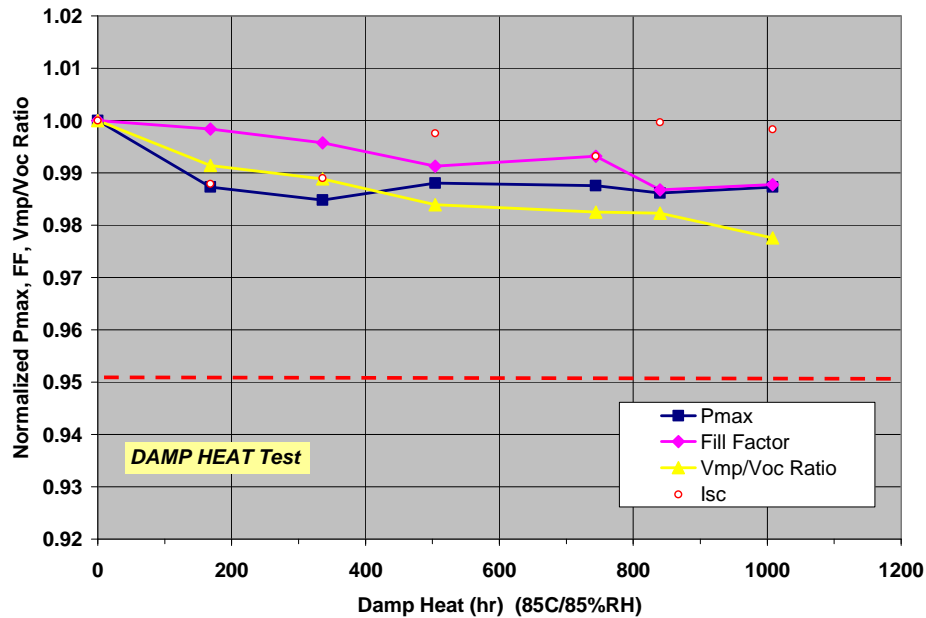


Figure 46. Results of damp heat tests for mini-module 08172007-04: 3x3 cell module with ribbon, conductive adhesive. The fraction drop in Pmax, fill factor, Vmp/Voc ratio, and Isc is shown over a period of 1008 hr. This sample performed favorably in the damp heat tests.

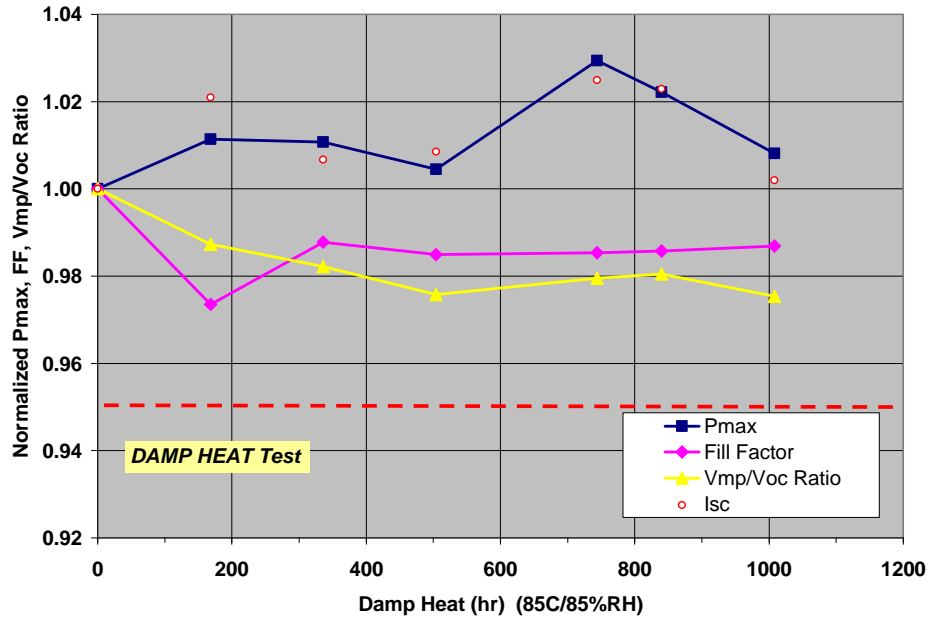


Figure 47. Results of damp heat tests for mini-module 7051608-4-8-18:1x3 cell module with ribbon, XCA80229HF conductive adhesive. The fraction drop in Pmax, fill factor, Vmp/Voc ratio, and Isc is shown over a period of 1008 hr. This sample performed favorably in the damp heat tests.

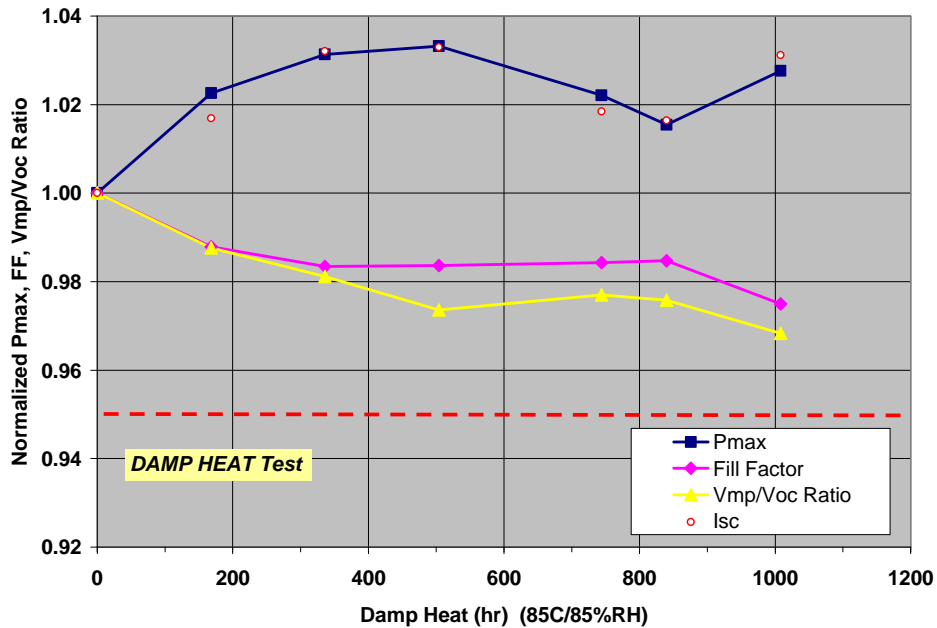


Figure 48. Results of damp heat tests for mini-module 7051607-4-5-6:1x3 cell module with ribbon, conductive adhesive. The fraction drop in Pmax, fill factor, Vmp/Voc ratio, and Isc is shown over a period of 1008 hr. This sample performed favorably in the damp heat tests.

CONCLUSION

- We reduced the quantity of screen-printed sintered Ag used for the grid metallization from 1.7 g/cell to 0.7 g/cell for a 125 mm × 125 mm cell. Extracting current from more places on the cell rear with copper ribbon attached to the gridlines enabled this. Thinning or narrowing the gridlines reduces Ag cost and wafer bowing.
- We reduced the “edge diode” series resistance, which is the series resistance in the Si above the screen-printed busbars and tabs of the basic edge-contacted EWT cells, as evidenced by fill factor improvement from around 0.70 to 0.74.
- We improved the performance of the cell by increasing the emitter coverage on the cell rear when the metallization width of the busbars was decreased and the screen-printed sintered Ag busbars was eliminated.
- We tested the electrical performance of busbarless cells with four probe methods that have been developed to date.
- Several hundred busbarless cells have been completed up through final metal print.
- COSMOS finite element analysis modeling was carried out on the busbarless cell design.
- Twelve-, nine-, six- and three-cell busbarless cell mini-modules were produced by manual assembly using the ribbon. Conversion efficiencies of the mini-modules were extremely favorable due to the significantly improved fill factor as made possible by the busbarless technology. Fill factors of the 12-cell mini-module showed the capability of exceeding 0.74 as compared to the 0.69 or 0.70 achieved for the conventional edge-tapped EWT cell modules. A nine-cell module efficiency of 14.5% was achieved with fill factor of 0.734.
- Testing of busbarless cells remains one of the more difficult issues to address. Analysis of the cells was carried out so that we could determine electrical properties (J_{sc} , V_{oc} , fill factor, shunt resistance, series resistance), and the mechanical properties of the interconnect were tested with the tab pull test.
- Five busbarless cell mini-modules were subjected to lifetime testing approximating the thermal cycling and damp heat tests approximating IEC 61215 conditions. The five mini-modules made with conductive adhesive and ribbon interconnects all passed these tests.

DISTRIBUTION

External Distribution:

20 Advent Solar, Inc.
Attn: James Gee
5600 University Blvd. SE
Albuquerque, NM 87106

Internal Distribution:

1 MS1033 Dan Riley, 6335
1 MS1033 Charles J. Hanley, 6335
1 MS1033 Jennifer E. Granata, 6335
1 MS1033 Michael A. Quintana, 6337
1 MS1110 Jeff Nelson, 6337
1 MS1110 Ward I. Bower, 6337
1 MS0899 Technical Library, 9536 (*electronic copy*)

